ChemComm

Chemical Communications

www.rsc.org/chemcomm

Number 18 | 14 May 2008 | Pages 2061–2168

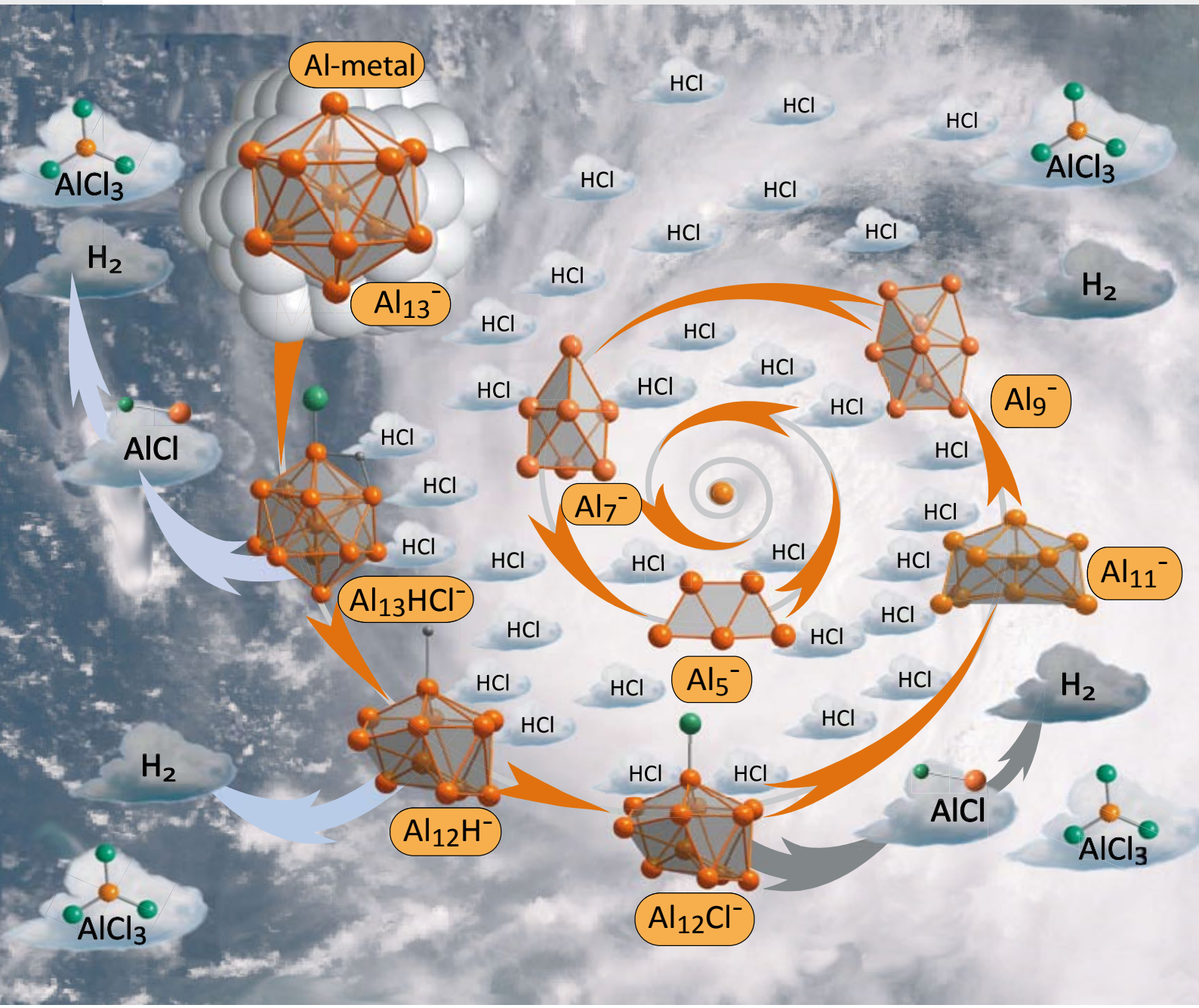

ISSN 1359-7345

RSC Publishing

FEATURE ARTICLE
Ralf Burgert and Hansgeorg Schnöckel
Monitoring the dissolution process of metals in the gas phase

FEATURE ARTICLE
Penelope J. Brothers
Boron complexes of porphyrins and related polypyrrole ligands: unexpected chemistry for both boron and the porphyrin

1359-7345(2008)18;1-1

Monitoring the dissolution process of metals in the gas phase: reactions of nanoscale Al and Ga metal atom clusters and their relationship to similar metalloid clusters†‡

Ralf Burgert and Hansgeorg Schnöckel*

Received (in Cambridge, UK) 22nd January 2008, Accepted 19th February 2008
First published as an Advance Article on the web 19th March 2008
DOI: 10.1039/b801224e

Formation and dissolution of metals are two of the oldest technical chemical processes. On the atomic scale, these processes are based on the formation and cleavage of metal–metal bonds. During the past 15 years we have studied intensively the intermediates during the formation process of metals, *i.e.* the formation of compounds containing many metal–metal bonds between naked metal atoms in the center and ligand-bearing metal atoms at the surface. We have called the clusters metalloid or, more generally, elementoid clusters. *Via* a retrosynthetic route, the many different Al and Ga metalloid clusters which have been structurally characterized allow us to understand also the dissolution process; *i.e.* the cleavage of metal–metal (M–M) bonds. However, this process can be detected much more directly by the reaction of single metal atom clusters in the gas phase under high vacuum conditions. A suitable tool to monitor the dissolution process of a metal cluster in the gas phase is FT-ICR (Fourier transform ion cyclotron resonance) mass spectrometry. Snapshots during these cleavage processes are possible because only every 1–10 s is there a contact between a cluster molecule and an oxidizing molecule (*e.g.* Cl_2). This period is long, *i.e.* the formation of the primary product (a smaller metal atom cluster) is finished before the next collision happens. We have studied three different types of reaction:

(1) Step-by-step fragmentation of a structurally known metalloid cluster allows us to understand the bonding principle of these clusters because in every step only the weakest bond is broken.

(2) There are three oxidation reactions of an Al_{13}^- cluster molecule with Cl_2, HCl and O_2 central to this review. These three reactions represent three different reaction types, (a) an exothermic reaction (Cl_2), (b) an endothermic reaction (HCl), and (c) a kinetically limited reaction based on spin conservation rules (O_2).

(3) Finally, we present the reaction of a metalloid cluster with Cl_2 in order to show that in this cluster only the central naked metal atoms are oxidized, and a smaller metalloid cluster results containing the entire protecting shell as the primary cluster.

All the experimental results, supported by quantum chemical calculations, give a rough idea about the complex reaction cascades which occur during the dissolution and formation of metals. Furthermore, these results cast a critical light on many simplifying and generalizing rules in order to

Universitat Karlsruhe, Institut fur Anorganische Chemie, Engesserstrasse, Karlsruhe, D-76128, Germany. E-mail: hg@chemie.uni-karlsruhe.de

† In memoriam Peter Timms.

‡ Electronic supplementary information (ESI) available: Additional figures. See DOI: 10.1039/b801224e

Ralf Burgert studied chemistry at the Technical University, Karlsruhe (Germany), where he obtained his PhD under the supervision of Prof. Schnöckel in 2007. His research activities focused on mass spectroscopic investigations of reactions of metal atom clusters. He left the university in 2007 to work as a laboratory team leader at Biologische Heilmittel Heel GmbH in Baden-Baden.

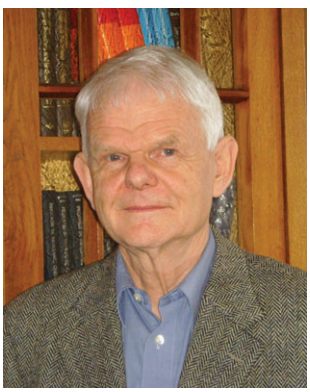

Hansgeorg Schnöckel gained his PhD (University of Münster) with H. J. Becher in 1970. He then began spectroscopic matrix investigations of reactive high-temperature molecules as the basis for later work. In 1987 he became professor and moved to the University of Munich in 1989. From 1993–2007 he held the chair of analytical chemistry at the University of Karlsruhe; he is now professor emeritus.

understand the bonding and structure of metal clusters. Finally, the experiments and some recent results provided by physical measurements on a crystalline Ga_{84} compound build a bridge to nanoscience; *i.e.* they may be a challenge for chemistry in the next decades, since it has been shown that only with a perfect orientation of nanoscale metal clusters, *e.g.* in a crystal, can novel, unexpected properties (*e.g.* superconducting nanoscale materials) be obtained.

1. Introduction

The dissolution of precious metals (*e.g.* Au, Ag),§ as well as the formation of base metals (*e.g.* Fe),¶ are among the oldest technical–chemical processes. Nevertheless, nearly nothing is known about the mechanism, *i.e.* about intermediates and single steps on an atomic scale. This at first surprising deficiency seems, however, to be plausible since there is a great number of these intermediates, some of them with an extremely short life time, although many processes occur during every reaction step, *e.g.* M–M bonds (M = metal) and M–X bonds (X = non-metal atoms, *e.g.* halogen or oxygen atoms) are formed and broken. In a hypothetical experiment, *e.g.* a constantly decreasing metal particle during a dissolution process, such intermediates can best be examined in a molecular shape, *i.e.* as clusters. Clusters exhibiting exclusively M–M bonds are called naked metal atom clusters (M_n) or simply metal atom clusters.[1,2] Normally, they are formed and investigated under high-vacuum conditions. On the other hand, there are metalloid cluster compounds (M_nX_m, $n > m$) which usually crystallize from solutions. These metalloid clusters—the *terminus technicus* was introduced by our group some time ago[3,4]—are characterized by the fact that the number of M–M bonds in the core exceeds the number of M–X bonds in the outer shell. In recent years, our research has focused on the synthesis and structural characterization of metalloid aluminium and gallium clusters, which can be regarded as intermediates on the way to the bulk metals.[5–10] To a certain extent, this interpretation is based on the synthesis of *e.g.* metalloid aluminium clusters *via* the metastable monohalides. Their disproportionation‖ (eqn (1)) towards bulk aluminium and aluminium trihalide as final products has turned out to be a suitable method because we have created low temperature conditions under which this process does take place, but in a controlled way. Thus, we obtained crystalline intermediates as snapshots of the formation of the metals. The average oxidation state, *e.g.*, of such metalloid Al clusters is expected to be between +1 (*e.g.* AlCl) and 0 (the metal). For example, the oxidation number of Al in the $Al_{77}R_{20}^{2-}$ cluster ion (R = bulky, negatively charged ligand $N(SiMe_3)_2$, see Fig. 1) is +0.23.[12]

$$3AlX_{(g)} \rightarrow 2Al_{(s)} + AlX_{3(g)} \qquad (1)$$

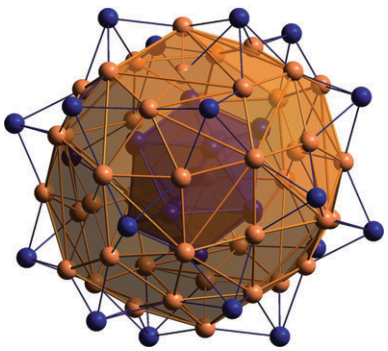

Fig. 1 The $[Al_{57}(AlR)_{20}]^{2-}$ cluster anion in the crystalline state and its arrangement of the 77 Al atoms: a central Al atom is surrounded by 12 Al atoms (between an icosahedral and cuboctahedral orientation), and then there is a second "shell" of 44 Al atoms. In the third "shell" there are 20 (blue) Al atoms which are directly bonded to the N atoms of the $N(SiMe_3)_2$ ligands. The Al–Al distances decrease from the centre to the outer shell (Al^+ is smaller than Al^0). With its 57 naked Al atoms, this cluster is one of the largest metalloid clusters.

The more adequate bonding description shows that a core of 57 "naked" Al atoms is stabilized by 20 carbenoid AlR moieties: $[Al_{57}(AlR)_{20}]^{2-}$ (*cf.* below). Formally—*i.e.* by neglecting the 20 negatively charged ligands—a cluster species has formed in which 57 Al atoms are already reduced to the oxidation state 0, *i.e.* to the metal, and where the outer shell consists exclusively of Al^+ ions: $[Al_{57}(Al^+)_{20}]^{18+}$.[13] This hypothetical cluster species can not only be regarded as a model for the formation of the metal itself, but may also serve as a model for the oxidation process, *i.e.* for the dissolution process of an Al_{77} moiety, as represented by a negatively charged Al_{77}^{2-} cluster:**

$$Al_{77}^{2-} \rightarrow 20e + [Al_{57}(Al^+)_{20}]^{18+}$$

How can this oxidation process comprising 20 electrons be divided into steps where only one or two electrons are involved, or, in other words, how can this process be observed in a time-resolved way? For this purpose, the oxidation of "naked" metal atom clusters has to be studied in the highly

§ "*Aqua regia*" was used for the first time in the 13th century in order to separate Au and Ag.

¶ The date of the full Iron Age, in which this metal for the most part replaced bronze in implements and weapons, varied geographically, beginning in the Middle East and southeastern Europe about 1200 BC.

‖ In order to get a solution of metastable aluminium monohalides, we have developed a highly sophisticated, technically non-trivial method which has been fruitfully applied for the past 20 years.[11]

** This interpretation of the bonding description of a metalloid cluster containing metal atoms of a base metal is based on bond energy reasons (*cf.* 3.2) and on the decreasing M–M distances from the centre to the outer oxidized shell, *i.e.* the oxidized atoms are, as expected, smaller. The situation in metalloid clusters of precious metals is completely different: there are increasing M–M distances from the centre to the outer shell;[14] these clusters consist of nearly electronically neutral (oxidation state 0) metal atoms which are expanded in the outer shell *via* ligand repulsion, *i.e.* there are no oxidized metal atoms, and therefore these clusters do not represent a model for the solution process of the metals. A more detailed comparison of two recently published Pd_{164}[14] and Au_{102}[15,16] cluster compounds with the metalloid clusters of Al and Ga has been presented in a further review.[17]

diluted gas phase where collisions between molecules occur relatively seldom. Then, snapshots of the dissolution process should be obtained (*e.g.* the first and second oxidation steps of an Al_n cluster to $Al_{n-1}Al^+$ and $Al_{n-2}(Al^+)_2$), and could be considered as molecular models for the dissolution of the metal.

The perfect tool for observing these elementary steps, though only applicable to charged $M_n^{\pm}$ species, is FT-ICR mass spectrometry (Fourier transform ion cyclotron resonance mass spectrometry), working under UHV (ultra-high vacuum) conditions. The cluster ions formed *via* different ionization methods (*cf.* below) exist in a highly diluted atmosphere ($<10^{-9}$ mbar); under these conditions, collisions between the cluster ions (Al_n^-) and the great excess of oxidizing molecules (*e.g.* Cl_2) take place only about every 10 s (*e.g.* eqn (2)).

$$Al_n^- + Cl_2 \rightarrow Al_{n-2}(AlCl)_2^- \rightarrow Al_{n-2}^- + 2AlCl \quad (2)$$

This is a very rough description of the first oxidation step of an Al_n^- cluster: during this first reaction step between two molecules taking place on an atomic scale, many changes result with respect to the topology of the atoms as well as to the electrons, *i.e.* the whole bonding situation is changed dramatically, for there are addition, elimination, and rearrangement steps involved, where bonds are formed and broken. Nevertheless, these primary steps (eqn (2)) are very fast (nanoseconds to milliseconds), especially when compared to the average time until the next collision of this cluster with Cl_2. Thus, *via* this mass spectrometric method, reaction steps between two single molecules can be detected as snapshots of a complex reaction cascade, finally leading to $AlCl_3$ ($AlCl + Cl_2$), and thus to the complete oxidation of all the atoms of this Al_n^- cluster.

Hereafter, the experimental details of the FT-ICR mass spectrometric investigations will be briefly described, and followed by examples in order to demonstrate the high potential of this method with respect to the objectives of this article. First, collision experiments with excited metalloid cluster ions will be presented, followed by several chemical reactions (Cl_2, HCl, O_2) of naked metal atom clusters in the main section. Finally, a description of the first oxidative degradation process of a structurally characterized metalloid cluster ion will be discussed. These last results will raise the question of whether or not Wade's rules,[18–20] which can be applied to the polyhedral boron subhalides, can also predict the ground state structures in the analogous aluminium and gallium compounds.

2. Mass spectrometry and quantum chemical calculations

The experiments were performed with a commercial FT-ICR mass spectrometer (IonSpec), equipped with a superconducting 7.0 T magnet and two different ion sources. By laser desorption/ionization (LDI), solid compounds were vaporized with a nitrogen laser (Spectra Physics, $\lambda = 337.1$ nm). Aluminium cluster anions Al_n^- were generated in this way by using lithium aluminium hydride ($LiAlH_4$) as the target (*cf.* below). On the other hand, electrospray ionization (ESI) proved to be one of the softest methods of transferring ions into the gas phase from polar solvents. By this means, even sensitive compounds containing cluster ions such as $Ga_{19}R_6^-$ [21] or $C@W_6Cl_{18}^{2-}$ [22] remained intact, *i.e.* showed no fragmentation. Under ultra-low pressure conditions (typically 10^{-10} mbar), ions were trapped in the ICR cell by strong magnetic and electric fields. With the high resolution of the instrument, even single isotopomers of the desired clusters could be isolated and detected in the ion trap. A pulsed valve was used to admit argon as the collision gas in order to cool ions to room temperature. SORI-CAD experiments (sustained off-resonance induced collisionally activated dissociation) were performed by excitation of selected cluster ions (by a radio frequency pulse) and in the presence of argon (using the pulsed valve). For studying reactions, the reactant gas, *e.g.* Cl_2, was introduced *via* a leak valve. This typically raised the pressure to 10^{-8} mbar. Because of the infrequency of collisions (one per 10 s) at low pressure, the complete reaction process was greatly slowed, and primary reactions steps were followed mass spectrometrically. Here the reaction products were detected in the range between 2 and 70 s.

It was not possible experimentally to determine reaction energies. Calculations were therefore carried out with the DFT-implementation of the TURBOMOLE[23] program package, using the Becke–Perdew-86 functional (BP86).[24,25] Coulomb interactions were treated within the RI (resolution of the identity) approximation.[26,27] The basis set was of split valence plus polarization (SVP) type.[28] To check whether the computational methods were suited to our tasks, we compared the following reactions: $AlCl_{(g)} + Cl_{2(g)} \rightarrow AlCl_{3(g)}$. The calculated reaction enthalpy was determined to be $\Delta_R H^{\ominus}$(calc) = -516 kJ mol^{-1}. The experimental value for the reaction energy is $\Delta_R H^{\ominus}$(exp) = -534 ± 9 kJ mol^{-1}.[29] In the past, these methods were also used in a density functional study of aluminium clusters.[30] In some cases (O_2 reactions), energies were calculated at a higher level of theory (CCSD(T)). In order to check alternative reaction channels (kinetics), the lifetimes of the intermediate steps $[Al_{13}Cl_2]^-$* and $Al_{12}Cl^-$* were estimated by phase space theory (PST).[31–33]

3. Collisionally induced fragmentation experiments on cluster ions exhibiting experimentally determined structures. The stepwise degradation of the clusters gives an insight into the stability of different metal–metal bonding within these moieties

After some former LDI experiments with the solid compounds $SiAl_{14}Cp^*_6$[34]‡ and $Al_4Cp^*_4$,[35] followed by SORI-CAD investigation in order to find the weakest bonds within the cluster ions, we checked our commercially available electrospray ionization (ESI) equipment.[34,35] We wanted to find out whether or not this setup was also suitable to detect cluster ions in stable solution. Therefore, we started with a chemically rather inert $C@W_6Cl_{18}$ cluster anion containing a carbon atom in the centre of its W_6 cage.[22,36,37] After these experiments had demonstrated that our ESI source was basically suitable for the realization of such investigations, we intended

to use this route for transferring the metalloid cluster ion $[Ga_{13}(GaR)_6]^-$[4,21] from the solution to the gas phase. Because of the high sensitivity of this cluster ion to moisture and air, however, serious problems occurred. We therefore constructed a new ESI source which could be conditioned before the experiment in order to avoid contamination (especially by H_2O). In the following paragraph, both experiments performed with the help of the new ESI source are described.††

3.1 Mass spectrometric investigations of the dissociation of $[C@W_6Cl_{17}]^-$ anions[22]

In the experiments described here, the cluster anion $[C@W_6Cl_{17}]^-$, **1**, is investigated in the gas phase after electrospray ionization (ESI) of a methanolic solution of $Li_2C@W_6Cl_{18}$ (which has been fully characterized by X-ray diffraction[36,37]). By loss of Cl^- from the dianion $C@W_6Cl_{18}^{2-}$, **1** is formed. Afterwards, the degradation of **1** was observed step-by-step in collisionally activated dissociation (CAD) experiments.[22]

In order to examine the stepwise fragmentation of this cluster species in the gas phase, several mass selection and dissociation experiments were performed. First, the most intense signal out of the great number of isotopomers of **1** could be identified at m/z = 1718. The fragmentation of **1** takes place after collisionally activated dissociation by RF-irradiation and admission of argon. Three new signal groups can be observed and assigned to the compounds $[C@W_5Cl_{13}]^-$, **2**, $[C@W_4Cl_9]^-$, **3**, and $[C@W_3Cl_6]^-$, **4**. In order to confirm experimentally that the dissociation of **1** is proceeding by a consecutive mechanism where WCl_4 is split off twice consecutively and WCl_3 once, the following procedure was applied: each of the species **2**, **3** and **4** was isolated again and dissociated by collisional activation. The resulting fragments proved to be both **3** and **4**, as well as only **4**. During the fragmentation of **4**, the appearance of only Cl^- is observed. Based on the multitude of experimental findings, the following reaction channel can be inferred (eqn (3)):

$$\begin{aligned}[C@W_6Cl_{17}]^-\mathbf{1} &\xrightarrow[\Delta E_1]{-WCl_4} [C@W_5Cl_{13}]^-\mathbf{2}\\ &\xrightarrow[\Delta E_2]{-WCl_4} [C@W_4Cl_9]^-\mathbf{3}\\ &\xrightarrow[\Delta E_3]{-WCl_3} [C@W_3Cl_6]^-\mathbf{4}\end{aligned} \quad (3)$$

These fragmentation processes are especially interesting as both WCl_4^- and WCl_3 are used as starting compounds for the synthesis of $[C@W_6Cl_{18}]^{n-}$.[39]

However, the dissociation pathway of **4** remains unclear, and it was not possible, moreover, to determine the fragmentation energy experimentally. In order to find answers to questions concerning the structure of the intermediates, as well as the energy balance during the dissociation processes, we performed density functional theory (DFT) calculations, giving an adequate basis for the discussion of the experimental results, *viz*. ΔE_1 = 196 kJ mol^{-1}, ΔE_2 = 63 kJ mol^{-1} and ΔE_3 = 256 kJ mol^{-1}.

The mass spectrometric methods used here cannot answer the question of the fragmentation of $[C@W_3Cl_6]^-$, **4**, since no further fragmentation to smaller $[C@W_xCl_y]^-$ units is observed. A plausible reaction channel could be a simple electron loss from **4**, since an electron affinity of 332 kJ mol^{-1} was calculated for $[C@W_3Cl_6]$. However, the exclusive detection of Cl^- in dissociation experiments of **4** hints at a different reaction channel. Under preparative conditions, as in the aforementioned synthesis of **1**, a reduction could be possible where—apart from Cl^-—only the neutral starting compounds emerge. For this hypothetical mode of dissociation we calculated an energy change of +306 kJ mol^{-1} (eqn (4)).

$$[C@W_3Cl_6]^- \rightarrow Cl^- + \tfrac{1}{4}WCl_4 + CCl_4 + 11/4\ W_{(s)} \quad (4)$$

The results obtained experimentally and *via* quantum chemical methods for the dissociation of **1** *via* **4** demonstrate that the smallest C-containing tungsten cluster $[C@W_3Cl_6]^-$ that is observed during the experiment is possibly one of the first clusters generated in syntheses starting from solid tungsten, WCl_4 and CCl_4 (*cf*. eqn (4)). Furthermore, the results here raise the questions in principle of the extent to which the insertion of a carbon atom in these clusters is reflected in the energy balance, and of how strongly the C atom is bound. We examined $C@W_4Cl_8$, which is similar to **3**, and calculated the energy needed to remove the carbon atom to be 699 kJ mol^{-1} (eqn (5)).

$$C@W_4Cl_8 \rightarrow C_{(g)} + W_4Cl_8 \quad (5)$$

The calculated energy gain from the insertion of a carbon atom into a molecular tungsten atom framework also corresponds to the experimentally determined value for the formation of solid tungsten carbide, WC, from tungsten metal and carbon atoms (752 kJ mol^{-1}).[29] Hence, the carbon-centred metal clusters like **1** are suitable molecular models for the topological and energetic situation within the appropriate solid compounds. Recent investigation of a similar compound containing nitrogen instead of carbon within the W_6 core has demonstrated the capability of FT-ICR mass spectrometric investigations (Fig. 2).[39,40]

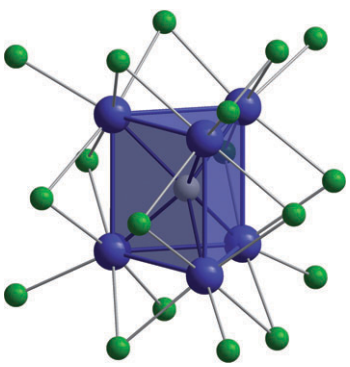

Fig. 2 The carbon-centred tungsten cluster anion $[C@W_6Cl_{18}]^{2-}$ (W blue, C grey, Cl green).

†† Further similar experiments with the metalloid $Ge_9R_3^-$ cluster (R = $Si(SiMe_3)_3$) exhibit a completely different fragmentation pattern, *i.e*. as expected, bonding, especially of the ligands, is different in Ga and Ge clusters.[38]

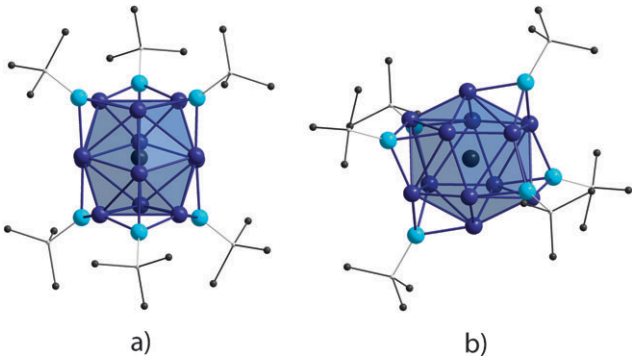

Fig. 3 Two different presentations of the $[Ga_{13}(GaR)_6]^-$ cluster (R = $C(SiMe_3)_3$). The 6 ligand-bearing Ga atoms are light-blue colored; the central Ga atoms are black. (a) The 3-fold axis of the cluster and the cuboctahedral-like presentation of the 13 central Ga atoms (there are two different types of Ga–Ga distances from the central Ga atom: 6 × 273 pm and 6 × 295 pm (to the three upper and lower triangles). (b) The distorted icosahedral arrangement within the Ga_{13} unit is highlighted.

3.2 The successive fragmentation of a structurally characterized metalloid cluster anion in the gas phase: $[Ga_{13}(GaR)_6]^- \rightarrow [Ga_{13}]^- + 6GaR$ (R = $C(SiMe_3)_3$)[21]

The crystalline compound containing the metal atom cluster $[Ga_{13}(GaR)_6]^-$ (Fig. 3) stands out from other metalloid cluster compounds, since it is soluble in organic solvents without decomposition.[4] As demonstrated above, electrospray ionization proved to be an appropriate method to transfer the ions from solutions into the gas phase. Thus, we were able for the first time to perform fragmentation reactions on a structurally characterized metalloid cluster in the gas phase. SORI-CAD experiments allowed us to induce fragmentation reactions resulting in the breaking of the weakest bonds, and demonstrated that carbenoid GaR units are split off one after another, until the naked Ga_{13}^- core is left (Fig. 4). These results were unexpected, since Ga–Ga bonds within the Ga_{13}^- core are significantly longer (274 pm) than the average distance between the ligand-bearing Ga atom and the neighbouring Ga atom of the cluster core (around 250 pm).[4] Nevertheless, the shortest bonds were observed to be broken, implying that the ensemble of GaR units containing oxidized Ga atoms‡‡ must be considered as a protecting ligand shell for the Ga_{13}^- core, in analogy to CO ligands for precious metal clusters. In order to describe the bonding situation, it could be demonstrated that $[Ga_{13}(GaR)_6]^-$ does *not* consist of a highly positively charged metal atom core (Ga_{19}^{5+}) that is surrounded by six negatively charged R^- units. Instead, the $[Ga_{13}(GaR)_6]^-$ cluster should be regarded as a ligand covered Ga_{13}^- ion which is an outstandingly stable cluster ion because of its closed shell configuration (jellium, 40 electrons, *cf.* below). Such an interpretation is in line with the high solubility of this compound, indicating that, beside Madelung interactions, there are no further interactions between $[Ga_{13}(GaR)_6]^-$ moieties within the crystal lattice.‡‡

‡‡ This behaviour is in contrast to the properties of neutral Al_7R_6 clusters (see ESI‡) described recently. There a strong electronic interaction between the Al_7R_6 species within the crystal lattice was found and therefore the cluster is stable only in the solid state, *i.e.* it decomposes during the attempts at dissolution in a solvent.[41,42]

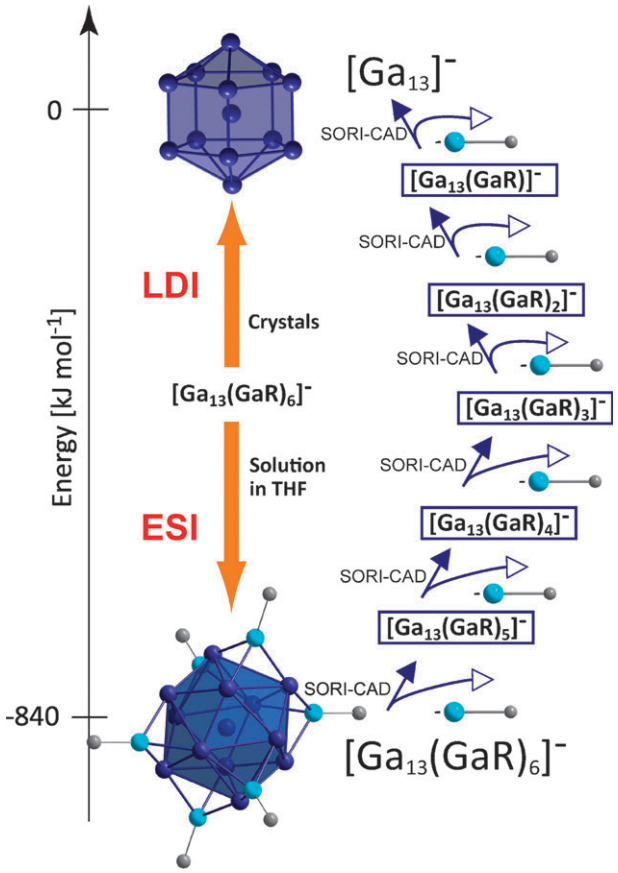

Fig. 4 By electrospray ionization (ESI), $[Ga_{13}(GaR)_6]^-$ clusters can be transferred entirely into the gas phase, *i.e.* without decomposition. Here the fragmentation pattern of the $[Ga_{13}(GaR)_6]^-$ cluster after collisionally induced dissociation (SORI-CAD) is displayed. Ga_{13}^- (which is the final reaction product) can also be obtained by laser desorption ionization (LDI) of crystals containing $[Ga_{13}(GaR)_6]^-$.

By laser desorption/ionization of solid crystals containing $[Ga_{13}(GaR)_6]^-$,[43] only Ga_n^- clusters were observed mass spectrometrically, with a dominant signal group that could be assigned to the pre-eminently stable Ga_{13}^-. All the GaR units were obviously lost during the laser vaporization process. Fig. 4 summarizes these results graphically. In any understanding of the structure of metalloid clusters, this series of dissociation reactions has to be called a key experiment. The FT-ICR MS experiments provide an excellent basis for the bonding description of the clusters, since the weakest bonds are revealed. In combination with quantum chemical calculations, the exploration of the fragmentation process leads to an experimentally based understanding of the bond properties of many of the recently investigated metalloid gallium and aluminium clusters.

4. Chemistry of naked Al_{13}^- ions

The results of the previous section demonstrated convincingly on the basis of collisionally induced fragmentation

experiments that the metalloid cluster $[Ga_{13}(GaR)_6]^-$ can shed its 6 GaR ligands leading finally to the Ga_{13}^- ion, outstanding for its stability. The analogous Al_{13}^- ion is expected to be similar with respect to its electronic energy, but the geometric structures are different. In contrast to the decahedral D_{5h} structure of Ga_{13}^-, the Al_{13}^- ion exhibits a centred icosahedral structure.§§¶¶ The geometric and electronic structures of Al_{13}^- have been discussed in many mass spectrometric and quantum chemical investigations.[47–50] The closed-shell structure of 40 valence electrons, corresponding to the jellium model, led to its designation as a "super-atom". Consequently, Al_{13}^- has been called a super-halide atom,[51,52] since the high electron affinity (EA) of neutral Al_{13} of 3.6 eV is similar to those found for chlorine and fluorine atoms: Cl = 3.6 eV, F = 3.4 eV‖‖. We have selected Al_{13}^- for our reaction studies as a suitable metal atom cluster of one of the lightest metals, exhibiting a geometry of the central atom not very different from the cuboctahedral geometry of the bulk metal itself. Therefore, the Al_{13}^- cluster and its chemical reactions should be investigated with the aim of determining whether or not Al_{13}^- may be a molecular model for the reactions of the bulk metal. A molecular model for any reaction on a solid surface would be an asset, because, *e.g.*, metal surfaces cannot be realistically reproduced with respect to the topology of atoms in the atomic range. *A priori*, this idea of a molecular model compound for reactions on metal surfaces seems to be utopian, since major differences between the reaction sequences of Cl_2 with Al_{13}^- and of Cl_2 with an Al surface are to be expected. The latter reaction, *i.e.* the reaction Cl_2 with any base metal, is an experiment performed by many a university student in his or her first year. When Cl_2 molecules come into contact with an Al surface, Al–Cl bonds are formed in an exothermic reaction. Simultaneously with the formation of many Al–Cl bonds, the temperature rises, and finally, at high temperatures, every further Cl_2 contact leads to the formation of $AlCl_3$, which is then eliminated into the gas phase, *i.e.* Al metal is vaporized in a Cl_2 atmosphere, and $AlCl_3$, as Al_2Cl_6, sublimes to the cooler parts of the reaction vessel.[53] At lower Cl_2 pressures (*e.g.* under vacuum conditions), the heated Al metal reacts to form AlCl molecules which are stable high-temperature species[11] (*cf.* below). Altogether, during the chlorination of Al metal, a variety of reactions proceed on the metal surface, depending markedly on the reaction conditions. In contrast to these very complex reaction sequences, the situation after a single collision of a Cl_2 molecule with an Al_{13}^- cluster should be much clearer and easier to understand. Under UHV conditions, the first reaction step of these two species should be to produce a highly vibrationally excited $Al_{13}Cl_2^-$ intermediate which spontaneously ejects two AlCl molecules to form the smaller Al_{11}^- cluster (*cf.* eqn (2)).

In contrast to these principal differences between the chlorination of Al_{13}^- and Al metal—*i.e.* only a few reaction steps *versus* a complex reaction cascade—there is, at least at first glance, a surprising similarity with respect to the thermodynamics of the reactions (eqn (6) and (7)):

$$Al_{13}^-{}_{(g)} + 3Cl_2 \rightarrow Al_{11}^- + 2AlCl_{3(g)}$$
$$\Delta_R H_{(0\ K)} = -1137\ kJ\ mol^{-1}\ (calculated) \quad (6)$$

$$2Al_{(s)} + 3Cl_2 \rightarrow 2AlCl_{3(g)}$$
$$\Delta_R H_{(0\ K)} = -1166\ kJ\ mol^{-1}\ (exp.\ found)^{29} \quad (7)$$

Since this similarity of an Al_n cluster to the bulk metal regarding thermodynamics applies only to the Al_{13}^- cluster, the very special electronic structure of this cluster (jellium model),[54–58] as well as its topological similarity concerning the coordination number, is critical. In both cases, a central Al atom is surrounded by 12 further Al atoms, icosahedrally arranged in Al_{13}^-, and cuboctahedrally in the metal. Therefore, the aforementioned reactions and reactions to be discussed later become plausible if the amount of energy necessary to remove two Al atoms from an Al_{13}^- cluster is compared with the energy change in the case of the bulk metal (eqn (8) and (9)):

$$Al_{13}^-{}_{(g)} \rightarrow Al_{11}^-{}_{(g)} + 2Al_{(g)}$$
$$\Delta_R H^{\ominus}{}_{(0\ K)} = +698\ kJ\ mol^{-1}\ (calculated) \quad (8)$$

$$2Al_{(s)} \rightarrow 2Al_{(g)}$$
$$\Delta_R H^{\ominus}{}_{(0\ K)} = +654 \pm 8\ kJ\ mol^{-1}\ (exp.\ found)^{29} \quad (9)$$

Taking into account the usual error margin of DFT calculations (*cf.* above), the energy needed for the removal of 2 Al atoms either from an Al_{13}^- cluster or from the bulk Al metal is almost identical. Here Al atoms form the energetically equivalent reference system, and therefore all reactions of Al_{13}^- clusters and Al metal—which will be discussed later—should be very similar with respect to their energy balance.

In the following reactions of Al_{13}^- it will be further demonstrated that, besides this thermodynamical similarity to the bulk, there are plausible reasons for believing that similar primary steps are involved in reactions of Al_{13}^- and in those on an Al surface, *i.e.* Al_{13}^- is a plausible molecular model for the reaction kinetics of elementary reaction steps on an Al surface.

4.1 The chlorination of the Al_{13}^- cluster and the stepwise formation of its intermediate products, Al_{11}^-, Al_9^-, and Al_7^-[59]

After laser desorption/ionization (LDI) of lithium aluminium hydride ($LiAlH_4$), a homologous series of Al_n^- cluster anions could be observed mass spectrometrically (Fig. 5). Each of these mass spectra was dominated by an intense signal at m/z = 350.8 which can be assigned to Al_{13}^-. In the experiments described here, Al_{13}^- ions were first mass-selected (SWIFT) in the Penning trap of an FT-ICR mass spectrometer, and then cooled using argon as a collision gas.[13,60]

Upon exposing Al_{13}^- ions to a chlorine atmosphere of approx. 10^{-8} mbar, new signals, attributed mainly to Al_{11}^-, Al_9^-, and Al_7^- (Fig. 6) were observed after several tens of

§§ A decahedral Al_{13} moiety builds up the centre of an $Al_{69}R_{18}$ cluster.[44]‡

¶¶ An icosahedral Al_{13} moiety seems to be unusual, since among the large number of metalloid Al clusters, only the $Al_{77}R_{20}$ cluster exhibits a distorted Al_{13} centre (between a cuboctahedral and an icosahedral arrangement[12] *cf.* Fig. 1). Actual icosahedral Al_{12} moieties without a central Al atom are, however, present only in the subhalide $Al_{22}Cl_{20}$.[45,46]‡

‖‖ The EA of Ga_{13} is calculated to be 3.4 eV.[43]

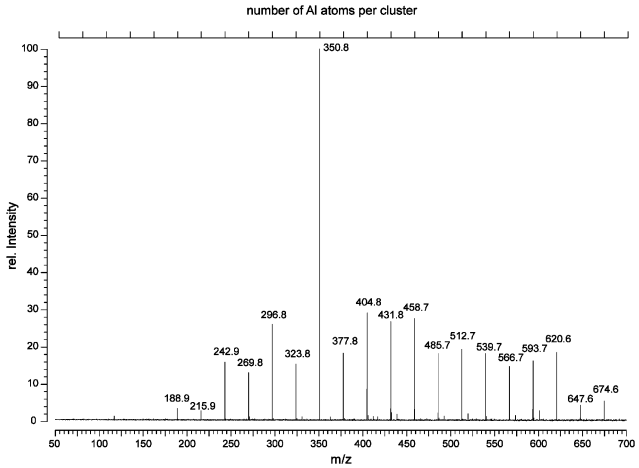

Fig. 5 Typical FT-ICR mass spectrum after laser-desorption/ionization of $LiAlH_4$. Here the distribution of aluminium cluster anions (Al_n^-) is displayed.

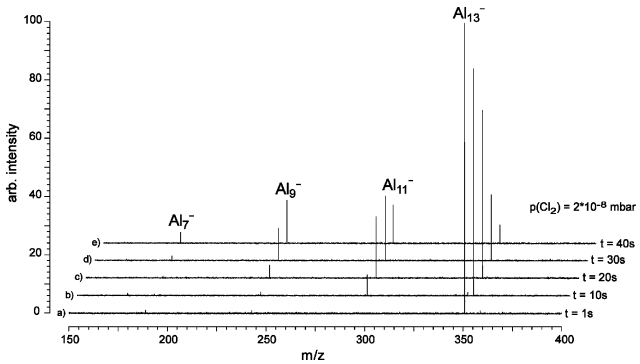

Fig. 6 Typical FT-ICR mass spectrum after laser desorption/ionization: at $t = 0$ s Al_{13}^- is isolated and exposed to a chlorine atmosphere (at 2×10^{-10} mbar). The decay of the Al_{13}^- signals in favour of Al_{11}^-, Al_9^-, and Al_7^- is presented.

seconds. These are due to the following stepwise reaction sequence (eqn (10)):

$$Al_{13}^- \xrightarrow[-2AlCl]{Cl_2} Al_{11}^- \xrightarrow[-2AlCl]{Cl_2} Al_9^- \xrightarrow[-2AlCl]{Cl_2} Al_7^- \qquad (10)$$

Based on our experimental observations and theoretical calculations, Fig. 7 summarizes the energetics of the stepwise elementary reactions that form these species. In the first step, oxidation of the Al_{13}^- cluster surface proceeds to form the intermediate product $[Al_{13}Cl_2]^-$*. The resulting reaction energy of this step is around -450 kJ mol^{-1}, according to density functional calculations. This leads to vibrational and rotational excitation energy trapped in the $[Al_{13}Cl_2]^-$* cluster that cannot be removed by collisions at pressures around 10^{-8} mbar (eqn (11a)). This, in turn, results in the fragmentation of $[Al_{13}Cl_2]^-$* into $Al_{12}Cl^-$ and AlCl in the next step (see eqn (11b)). Phase space theory[31–33] predicts a lifetime of several nanoseconds for $[Al_{13}Cl_2]^-$*, and as a consequence $[Al_{13}Cl_2]^-$* is not detected in the experiment. In the next step, $Al_{12}Cl^-$* also fragments, ejecting AlCl once again and leaving Al_{11}^- (see eqn (11c)). For this reaction channel, the lifetime of $Al_{12}Cl^-$* is estimated to be several tenths of a second. The Langevin rate constant k_L for all ion molecule reactions was determined to be $k_L = 0.09$ s^{-1} in the pressure range described.[61,62] As a consequence, an Al_n^- cluster molecule collides with a chlorine molecule every 10 s on average, and these will react to form an Al_{n-2}^- cluster within another 0.1 s, according to our lifetime estimates.

$$Al_{13}^-{}_{(g)} + Cl_2 \rightarrow [Al_{13}Cl_2]^-{}_{(g)} \quad \Delta_R H^{\ominus}{}_{(0\ K)} = -450\ kJ\ mol^{-1} \qquad (11a)$$

$$[Al_{13}Cl_2]^-{}_{(g)} \rightarrow Al_{12}Cl^-{}_{(g)} + AlCl_{(g)} \quad \Delta_R H^{\ominus}{}_{(0\ K)} = +195\ kJ\ mol^{-1} \qquad (11b)$$

$$Al_{12}Cl^-{}_{(g)} \rightarrow Al_{11}^-{}_{(g)} + AlCl_{(g)} \quad \Delta_R H^{\ominus}{}_{(0\ K)} = +187\ kJ\ mol^{-1} \qquad (11c)$$

In summary, the standard energy of reaction for Al_{13}^- breaking down to Al_{11}^- through its reaction with chlorine is -68 kJ mol^{-1}. In principle, the corresponding reactions of Al_{11}^- and Al_9^- are taking place in the same way. Their reaction energies are, however, -176 kJ mol^{-1} and -279 kJ mol^{-1}, respectively, these values being significantly more exothermic than for the $Al_{13}^- \rightarrow Al_{11}^-$ process. However, this is in agreement with the fact that smaller aluminium clusters exhibit weaker Al–Al bonds.***†††[64] Fig. 7 summarizes all of the pertinent energy balances. Beside the thermodynamic properties, rate constants have also been determined for the reactions of Al_{13}^-, Al_{11}^-, and Al_9 with chlorine.[32]

The reaction path presented here for the interaction of Al_n^- cluster ions with chlorine, resulting in the release of AlCl as the main product, is a plausible model for the corresponding reaction of bulk aluminium metal and chlorine. This conclusion is in accordance with other experiments as well. The chlorination of aluminium, as studied in matrix-isolation experiments, as well as in experiments on a synthetic scale, proceeds at high temperature and low chlorine pressures with the formation of AlCl.[65] The reaction paths deduced from mass spectrometric investigations with Al_n^- clusters provide a reasonable model for the primary steps during the oxidation of bulk aluminium. Moreover, the similarities between the bulk metal and Al_{13} clusters for the removing of two Al atoms (698 kJ mol^{-1} and 654 kJ mol^{-1}, see above) are consequently reflected in the corresponding chlorination reactions (eqn (12a, b and c)). The neutral Al_{13}, as well as the investigated anionic Al_{13}^- cluster can thus be considered as well-matched model compounds for investigations of primary reactions on the surface of bulk aluminium.

$$Al_{13}^-{}_{(g)} + Cl_2 \rightarrow Al_{11}^-{}_{(g)} + 2AlCl_{(g)} \quad \Delta_R H^{\ominus}{}_{(0\ K)} = -68\ kJ\ mol^{-1} \qquad (12a)$$

*** $Al_{13}^- \rightarrow Al_{11}^- + 2Al$, $\Delta_R H^{\ominus} = 698$ kJ mol^{-1}; $Al_{11}^- \rightarrow Al_9^- + 2Al$, $\Delta_R H^{\ominus} = 585$ kJ mol^{-1}; $Al_9^- \rightarrow Al_7^- + 2Al$, $\Delta_R H^{\ominus} = 480$ kJ mol^{-1}.

††† It should be mentioned that the structures of bare Al_9^- and Al_7^- clusters do not exhibit any symmetry elements and are therefore different from the arrangement within the $SiAl_8$ and Al_7 cluster core of ligand-stabilized $SiAl_{14}Cp_6$* (Si within a cube of 8 Al atoms)[63] and Al_7R_6[41] (D_{3d} symmetry in analogy to aluminium metal).‡

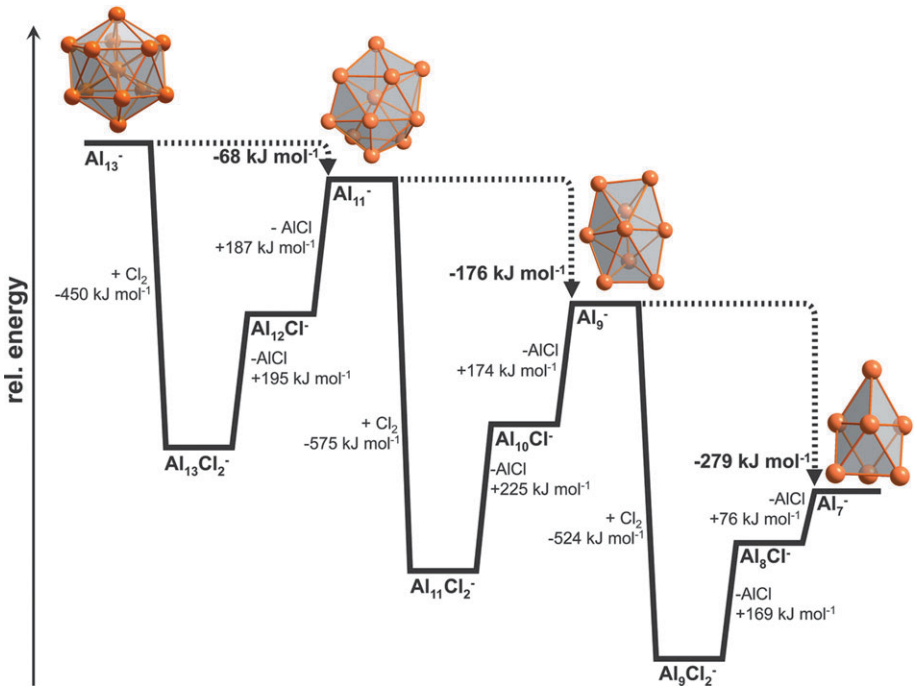

Fig. 7 Schematic energy diagram for the cluster degradation; the energy values are given in kJ mol^{-1}. In the first step, chlorine reacts with the surface of the Al_{13}^- cluster to form an $Al_{13}Cl_2^-$ cluster, which cannot be detected in the experiment because of its short lifetime. In the second step, the spontaneous fragmentation of $Al_{13}Cl_2^-$ leads to the release of AlCl and the formation of $Al_{12}Cl^-$*. Subsequent release of AlCl leads to Al_{11}^-. The degradation of Al_{11}^- and Al_9^- proceeds in the same manner.

$$2Al_{(s)} + Cl_2 \rightarrow 2AlCl_{(g)}$$
$$\Delta_R H^{\ominus}_{(0\ K)} = -103 \pm 12\ kJ\ mol^{-1} \quad (12b)$$

$$Al_{13(g)} + Cl_2 \rightarrow Al_{11(g)} + 2AlCl_{(g)}$$
$$\Delta_R H^{\ominus}_{(0\ K)} = -113\ kJ\ mol^{-1} \quad (12c)$$

It follows that the chlorination of bulk aluminium metal must also proceed primarily by the addition of chlorine and the release of AlCl. Then the subsequent reaction from AlCl to $AlCl_3$ will take place with the release of a reaction energy that is ten times higher (-534 kJ mol^{-1}). Consequently, the cumulative reactions (eqn (13a, b and c)), which yield $AlCl_3$ as the final product, reflect the character of Al_{13}^- as a molecular model for the bulk metal:

$$Al_{13}^{-}{}_{(g)} + 3Cl_2 \rightarrow Al_{11}^{-}{}_{(g)} + 2AlCl_{3(g)}$$
$$\Delta_R H^{\ominus}_{(0\ K)} = -1084\ kJ\ mol^{-1} \quad (13a)$$

$$2Al_{(s)} + 3Cl_2 \rightarrow 2AlCl_{3(g)}$$
$$\Delta_R H^{\ominus}_{(0\ K)} = -1166 \pm 6\ kJ\ mol^{-1} \quad (13b)$$

$$Al_{13(g)} + 3Cl_2 \rightarrow Al_{11(g)} + 2AlCl_{3(g)}$$
$$\Delta_R H^{\ominus}_{(0\ K)} = -1145\ kJ\ mol^{-1} \quad (13c)$$

4.2 Primary reaction steps of Al_{13}^- clusters in an HCl atmosphere[66]

By the reaction of hydrogen chloride (HCl) gas with bulk aluminium, aluminium chloride and hydrogen are formed. This reaction can also be studied on a molecular level under ultra-low pressure conditions in order to elucidate the single steps by which it proceeds. By admission of hydrogen chloride (HCl) to a distribution of aluminium cluster anions (Al_n^-), new signals appeared that could be assigned as $Al_{14}H^-$, $Al_{15}H^-$, and $Al_{16}H^-$ at pressures around 10^{-8} mbar, indicating that, *e.g.*, Al_{15}^- and HCl react to form $Al_{14}H^-$ and AlCl. In contrast to this, Al_{13}^- ions did not react spontaneously in the presence of HCl; the initial signal of isolated Al_{13}^- ions in the mass spectrum remained strong. However, when the kinetic energy of Al_{13}^- was increased by applying a radio frequency (RF) pulse, new signals occurred that could be assigned to $Al_{12}H^-$, $Al_{12}Cl^-$, $Al_{11}H_2^-$ and Al_{11}^- (see Fig. 8). When only short RF pulses ($\sim$5 s) were applied, the formation of $Al_{12}H^-$ (see Fig. 8b) was observed, whereas when slightly longer pulses ($\sim$15 s) were applied, Al_{11}^- also came clearly into view (see Fig. 8c). When still more energy was

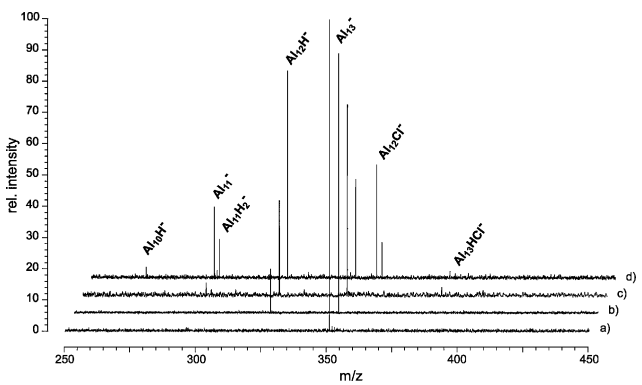

Fig. 8 After laser desorption/ionization of solid $LiAlH_4$, Al_n^- clusters are generated. Al_{13}^- is cooled by argon collisions, isolated, and exposed to an HCl atmosphere at 10^{-8} mbar. (a) Without external energy supplied (RF excitation), no reaction is observed. (b–d) When a little energy is supplied (irradiation with RF pulse length $\sim$5 s), $Al_{12}H^-$ and further reaction products are formed.

supplied (through longer pulse lengths of up to 40 s), all of the reaction products shown in eqn (14) and (15) appeared (see Fig. 8d). To specify further the reaction pathway, we isolated $Al_{12}H^-$ and let it react with HCl; both $Al_{12}Cl^-$ and $Al_{11}H_2^-$ resulted. The reaction of Al_{13}^- plus HCl can therefore be subdivided into two branches (eqn (14) and (15)):

$$Al_{13}^- \xrightarrow[-AlCl]{+HCl} Al_{12}H^- \xrightarrow[-H_2]{+HCl} Al_{12}Cl^- \xrightarrow[-AlCl]{} Al_{11}^- \quad (14)$$

$$Al_{12}H^- \xrightarrow[-AlCl]{HCl} Al_{11}H_2^- \xrightarrow[-H_2]{} Al_{11}^- \quad (15)$$

In each case, the reaction enthalpy has been calculated by density functional theory (DFT) methods.

$$Al_{13}^- + HCl \rightarrow [Al_{13}HCl^-]$$
$$\Delta_R H^{\ominus}_{(0\ K)} = -168\ kJ\ mol^{-1} \quad (16.1)$$

$$[Al_{13}HCl^-] \rightarrow Al_{12}H^- + AlCl$$
$$\Delta_R H^{\ominus}_{(0\ K)} = +217\ kJ\ mol^{-1} \quad (16.2)$$

$$Al_{12}H^- + HCl \rightarrow [Al_{12}H_2Cl^-]$$
$$\Delta_R H^{\ominus}_{(0\ K)} = -192\ kJ\ mol^{-1} \quad (16.3)$$

$$[Al_{12}H_2Cl^-] \rightarrow Al_{12}Cl^- + H_2$$
$$\Delta_R H^{\ominus}_{(0\ K)} = +30\ kJ\ mol^{-1} \quad (16.4a)$$

$$Al_{12}Cl^- \rightarrow Al_{11}^- + AlCl$$
$$\Delta_R H^{\ominus}_{(0\ K)} = +202\ kJ\ mol^{-1} \quad (16.5a)$$

$$[Al_{12}H_2Cl^-] \rightarrow Al_{11}H_2^- + AlCl$$
$$\Delta_R H^{\ominus}_{(0\ K)} = +118\ kJ\ mol^{-1} \quad (16.4b)$$

$$Al_{11}H_2^- \rightarrow Al_{11}^- + H_2$$
$$\Delta_R H^{\ominus}_{(0\ K)} = +114\ kJ\ mol^{-1} \quad (16.5b)$$

Overall, the reaction of Al_{13}^- plus HCl going to Al_{11}^-, H_2 and AlCl is seen to be endothermic:

$$Al_{13}^- + 2HCl \rightarrow H_2 + 2AlCl + Al_{11}^-$$
$$\Delta_R H^{\ominus}_{(0\ K)} = +89\ kJ\ mol^{-1} \quad (17)$$

The formation of an $[Al_{13}HCl^-]$ complex is postulated to be the first step during the reaction of Al_{13}^- with HCl (eqn (16.1)). As a consequence of the ultra-low pressure conditions, there is no bath gas to absorb its heat of formation (for $[Al_{13}HCl^-]$ $\Delta_R H_{(0\ K)} = -168$ kJ mol^{-1} as calculated by DFT). Therefore, since the exothermicity of the $[Al_{13}HCl^-]$* intermediate is so large, it is highly rotationally and vibrationally excited, and thus has a very short lifetime with respect to either dissociation back to the reactants or the dissociation channel shown in eqn (16.2). Since the dissociation to $Al_{12}H^-$ and AlCl (eqn (16.2)) was calculated to be endothermic by +217 kJ mol^{-1}, this event can proceed only if additional energy is supplied, *e.g.*, by RF excitation. If no additional energy is supplied, $[Al_{13}HCl^-]$* can only decompose back to the reactants, Al_{13}^- and HCl. This may be the reason why Al_{13}^- ions appear to be inert in an HCl atmosphere unless excitation is provided. With RF excitation, however, the charged reaction products of eqn (16.2) are observed.

The time between the collisions of the ions with HCl molecules at a pressure of 10^{-8} mbar is about 10 s on average, as deduced from the Langevin ion molecule reaction rate, where k_L is 0.11 s^{-1}.[61] In contrast to this long period between each collision, the respective reaction decay time of some of these cluster species is very short; phase space theory (PST) predicts the lifetimes of the product species $[Al_{13}HCl^-]$, $[Al_{12}H_2Cl^-]$, and $Al_{12}Cl^-$ to be only some few tenths of a second.[31,59] Considering the whole reaction cascade, the endothermic steps which lead to the products AlCl and H_2 are key steps in the mechanism. These steps are depicted in eqn (16.2, 16.4b and 16.5a) and in eqn (16.4a and 16.5b), corresponding to the elimination of the stable, high-temperature molecule AlCl and the generation of hydrogen gas (H_2), respectively. The formation of hydrogen proceeds *via* two different elimination reactions: in eqn (16.4a), Al–H and H–Cl bonds are broken and Al–Cl and H–H bonds are formed, while in eqn (16.5b), two Al–H bonds are broken and one H–H bond is formed.

All considered, the reaction of Al_{13}^- and HCl to give AlCl and Al_{11}^- is endothermic (+89 kJ mol^{-1} as estimated by DFT). Moreover, most of the elementary steps in the degradation of Al_{13}^- to Al_{11}^- (see eqn (16.1–16.5b)) are themselves endothermic. Their endothermicities and the ability to control RF excitation (energy input) permit the reaction to be stopped between steps, facilitating the direct detection of intermediate species. The reaction can then be started again at will by applying appropriate RF excitation. As compared with the reactions of other aluminium cluster anions and HCl, where many of the elementary steps appear to be exothermic, Al_{13}^- is a fortuitous case for mechanistic study. Its reaction pathway with HCl can be followed and mapped with fewer of the complications that might occur in other cases.

Furthermore, but of no less fundamental interest, the results presented here may be able to give a molecular interpretation for the well known differences between base and precious metals in an HCl atmosphere. While base metals are oxidized with the formation of the metal chloride, *e.g.* $AlCl_3$ and hydrogen, precious metals do not react with HCl. Thus, it seems plausible that the model reactions for Al_{13}^- in an HCl atmosphere should be different from the reactions of comparable centred clusters of a precious metal like gold. Consequently, these investigations, which should be seen as a challenge for the future, are a worthwhile pursuit in order to understand the fundamental differences between base and precious metals on a molecular level.

4.3 The reactivity of the Al_{13}^- cluster anion with triplet and singlet oxygen. The role of spin-conservation, an experimental proof[67]

When aluminium cluster anions Al_n^- (or cations) are exposed to oxygen, cluster ions with an odd number of aluminium atoms react significantly slower with O_2 than do those with an even number of aluminium atoms (see Fig. 9).

To facilitate this odd/even effect, mass-selected Al_{13}^- clusters were exposed to an O_2 atmosphere at 10^{-8} mbar in order to study their reactivity. Even after 600 s, essentially no reaction products were observed, and the initial Al_{13}^- signal remained strong (eqn (18)). On the other hand, mass-selected Al_{14}^- clusters reacted spontaneously under the same conditions to give Al_{10}^- and two Al_2O molecules (eqn (19)).

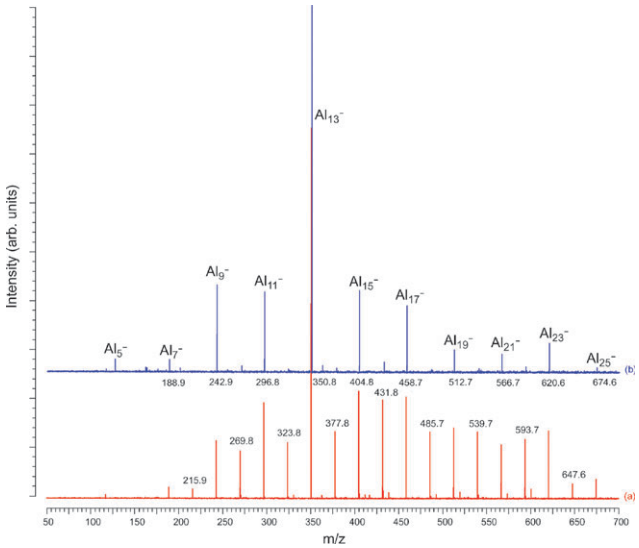

Fig. 9 Typical FT-ICR mass spectrum after laser-desorption/ionization of $LiAlH_4$. (a) The distribution of aluminium cluster anions (Al_n^-) is displayed (directly after cluster generation). (b) In the presence of oxygen all the Al_{even}^- anions are etched away (after 50 s at pressures around 9×10^{-9} mbar).

Obviously, the reaction of Al_{13}^- plus triplet oxygen (denoted in the following by $^{\uparrow\uparrow}O_2$) is extremely slow.

$$Al_{13}^-{}_{(g)} + {}^{\uparrow\uparrow}O_2 \nrightarrow Al_9^-{}_{(g)} + 2Al_2O_{(g)} \quad \text{(very slow reaction)} \qquad (18)$$

$$Al_{14}^-{}_{(g)} + {}^{\uparrow\uparrow}O_2 \rightarrow Al_{10}^-{}_{(g)} + 2Al_2O_{(g)} \qquad (19)$$

Although Al_{13}^- is a "double magic" cluster (40 electrons fulfil the jellium-like shell model,[57,58,68] and the topology represents a centred icosahedron[14]), and thus of particular interest, analogous findings were also encountered for reactions of other odd- and even-numbered clusters with O_2. Generally speaking, all Al_{odd}^- clusters react significantly more slowly with triplet oxygen than do Al_{even}^- clusters.

Spin conservation. To elucidate the described odd/even effect for Al_n^- clusters, we investigated the influence of spin conservation,[69] since spin influences have already been described for reactions between O_2 and aluminium surfaces.[69–74] Here the role of spin is highlighted by analyzing the reactions of Al_{13}^- and Al_{14}^- with triplet O_2 ($^{\uparrow\uparrow}O_2$). With its 40 valence electrons (closed shell), the spin multiplicity of the ground state of the Al_{13}^- cluster is a singlet (in the following labeled by $^{\downarrow\uparrow}Al_{13}^-$). Correspondingly, $^{\uparrow}Al_{14}^-$ has a doublet ground state due to its one unpaired electron. Looking more closely at the reaction steps during O_2 attack, we find that an initial adduct is formed where $^{\uparrow\uparrow}O_2$ is associated on the cluster surface (denoted, *e.g.*, by $^{\uparrow\uparrow}[Al_{13}{\cdot}O_2]^-$). Therefore, eqn (18 and 19) can be dissected into the following primary steps (eqn (18a and 19a)):

$$^{\downarrow\uparrow}Al_{13}^- + {}^{\uparrow\uparrow}O_2 \rightarrow {}^{\uparrow\uparrow}[Al_{13}{\cdot}O_2]^- \quad -0.36\ \text{eV} \qquad (18a)$$

$$^{\uparrow}Al_{14}^- + {}^{\uparrow\uparrow}O_2 \rightarrow {}^{\uparrow}[Al_{14}{\cdot}O_2]^- \quad -2.76\ \text{eV} \qquad (19a)$$

As a result of spin conservation restrictions,[75] $^{\uparrow\uparrow}[Al_{13}{\cdot}O_2]^-$ is formed in a triplet state and $^{\uparrow}[Al_{14}{\cdot}O_2]^-$ in a doublet state, *i.e.* they are spin-allowed. Subsequently, any further reaction of these adducts, in which the oxygen molecule dissociates on the surface of the cluster, causing heating, and leading to fragmentation of the cluster, may be accompanied by a barrier and, if necessary, by a spin-flip process (eqn (18b and 18c)).

$$^{\uparrow\uparrow}[Al_{13}{\cdot}O_2]^- \rightarrow\!\rightarrow {}^{\downarrow\uparrow}Al_{13}O_2^- \quad \text{spin transition and formation of covalent Al–O bonds} \qquad (18b)$$

$$^{\downarrow\uparrow}Al_{13}O_2^- \rightarrow {}^{\downarrow\uparrow}Al_9^- + 2Al_2O \qquad (18c)$$

For $^{\uparrow\uparrow}[Al_{13}{\cdot}O_2]^-$ this barrier is well defined: it is the crossing point of the triplet/singlet potential energy surface (PES), since the final fragments, Al_9^- and Al_2O, are both singlets. In addition to this barrier, there must be a spin-flip for $^{\uparrow\uparrow}[Al_{13}{\cdot}O_2]^-$, which in this case may have a low probability since the required spin–orbit coupling in the case of light metals like aluminium is expected to be small.[75]

The direct formation of $^{\downarrow\uparrow}[Al_{13}{\cdot}O_2]^-$ (singlet state) from Al_{13}^- and $^{\uparrow\uparrow}O_2$ is spin-forbidden (eqn (18d)).

$$^{\downarrow\uparrow}Al_{13}^- + {}^{\uparrow\uparrow}O_2 \nrightarrow {}^{\downarrow\uparrow}[Al_{13}{\cdot}O_2]^- \quad \text{spin forbidden} \qquad (18d)$$

In the case of Al_{14}^-, on the other hand, no such spin transition needs to occur since the initially formed $^{\uparrow}[Al_{14}{\cdot}O_2]^-$ can react without spin restrictions *via* $^{\uparrow}Al_{14}O_2^-$ to form the products $^{\uparrow}Al_{10}^-$ and Al_2O (eqn (19b and 19c)).

$$^{\uparrow}[Al_{14}{\cdot}O_2]^- \rightarrow\!\rightarrow {}^{\uparrow}Al_{14}O_2^- \quad \text{formation of covalent Al–O bonds} \qquad (19b)$$

$$^{\uparrow}Al_{14}O_2^- \rightarrow {}^{\uparrow}Al_{10}^- + 2Al_2O \qquad (19c)$$

We therefore hypothesize that reactions of aluminium clusters with odd n and $^{\uparrow\uparrow}O_2$ are expected to show diminished rates if the initially formed O_2 adduct is a triplet and the final products are singlets.

Reactions of Al_{13}^- and singlet O_2. In order to substantiate this idea experimentally, we manipulated the spin state of the aluminium-containing reactants by preparing aluminium hydride cluster anions, Al_nH^-,[76] and exposing them to $^{\uparrow\uparrow}O_2$ (the relevant experiments are not presented here).‡‡‡ Furthermore, we changed the spin of O_2 by generating singlet oxygen ($^{\downarrow\uparrow}O_2$), and allowing it to react with Al_{13}^- and other odd Al_n^- clusters.

In the reaction of Al_{13}^- with $^{\downarrow\uparrow}O_2$, the primary product $^{\downarrow\uparrow}[Al_{13}{\cdot}O_2]^-$ in its singlet state is expected to be formed (eqn (20a)). In the course of further reactions going through $^{\downarrow\uparrow}Al_{13}O_2^-$ (where O atoms are covalently bound) to the products, Al_9^- and two Al_2O molecules, all the reaction steps are spin-allowed (eqn (20b and 20c)).

$$^{\downarrow\uparrow}Al_{13}^- + {}^{\downarrow\uparrow}O_2 \rightarrow {}^{\downarrow\uparrow}[Al_{13}{\cdot}O_2]^- \quad -3.16\ \text{eV} \qquad (20a)$$

$$^{\downarrow\uparrow}[Al_{13}{\cdot}O_2]^- \rightarrow {}^{\downarrow\uparrow}Al_{13}O_2^- \quad \text{formation of covalent Al–O bonds } -4.53\ \text{eV} \qquad (20b)$$

$$^{\downarrow\uparrow}Al_{13}O_2^- \rightarrow {}^{\downarrow\uparrow}Al_9^- + 2Al_2O \quad -3.60\ \text{eV} \qquad (20c)$$

In comparison to reactions with $^{\uparrow\uparrow}O_2$, no spin transition is needed, and therefore no deceleration of the reaction is

‡‡‡ All $Al_{odd}H^-$ reacted rapidly with $^{\uparrow\uparrow}O_2$, whereas $Al_{even}H^-$ proved inert. Thus the reactivity pattern was dramatically inverted relative to the behaviour of Al_n^-, *e.g.* $Al_{13}H^-$ reacted, even though Al_{13}^- (and $Al_{13}H_2^-$) had been relatively unreactive, whereas the initial $Al_{14}H^-$ signal remained unchanged, while the Al_{14}^- signal decayed.[67,77]

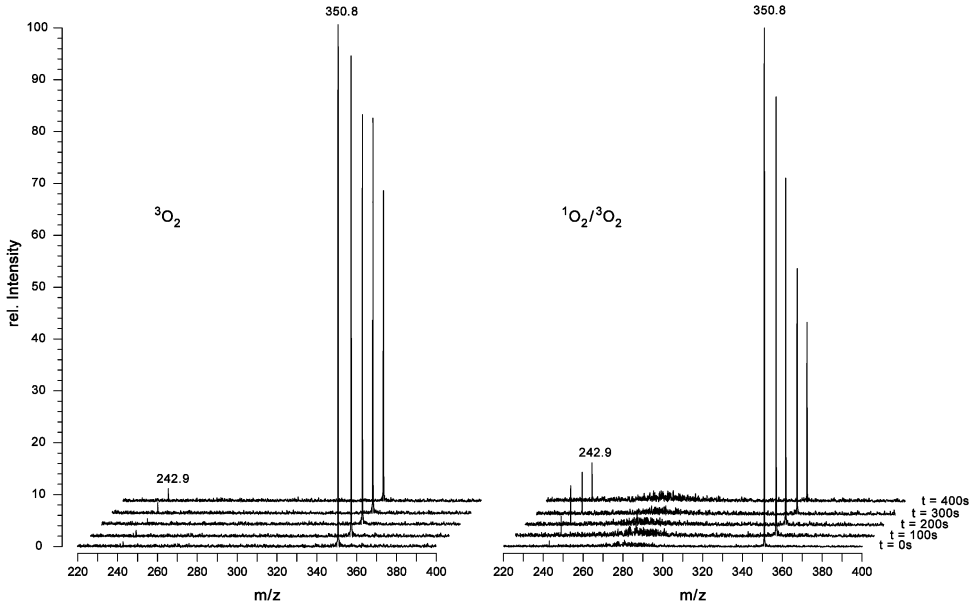

Fig. 10 Reactions of mass-selected Al_{13}^- clusters with $^{\uparrow\uparrow}O_2$ (left) and an $^{\downarrow\uparrow}O_2/^{\uparrow\uparrow}O_2$ mixture (right) by comparison. The FT-ICR mass spectra show Al_9^- as the only significant reaction product at m/z = 242.9 after 100–400 s of $^{\uparrow\uparrow}O_2$ and $^{\downarrow\uparrow}O_2/^{\uparrow\uparrow}O_2$ exposure.

expected. In order to prove this experimentally, $^{\downarrow\uparrow}O_2$ was generated by exposing $^{\uparrow\uparrow}O_2$ to a static electrical discharge (from a Tesla coil).[78] In this way, a $^{\downarrow\uparrow}O_2/^{\uparrow\uparrow}O_2$ mixture was obtained with an estimated $^{\downarrow\uparrow}O_2$ fraction around 5–10%. The $^{\uparrow\uparrow}O_2$ excess did not affect the experiment, since, according to Fig. 10 (left), the reaction of Al_{13}^- with $^{\uparrow\uparrow}O_2$ is significantly slower. Only $^{\downarrow\uparrow}O_2$ molecules react at a significant rate with Al_{13}^-, and Al_9^- would be expected as the only product. As shown in Fig. 10 (right), Al_{13}^- is indeed degraded to Al_9^- in an $^{\downarrow\uparrow}O_2$-containing atmosphere. The companion figure (Fig. 10, left) shows the effect of exposing Al_{13}^- to pure $^{\uparrow\uparrow}O_2$.

Calculations and conclusions. Quantum chemical calculations support our experimental findings. Fig. 11 summarizes most of the data from our calculations. In order to model the odd/even effect, we assumed that the overall reaction, where an Al_n^- cluster is degraded to a smaller fragment by oxygen, is a multi-stage process. In the initial step O_2 interacts with the cluster to form an 'adduct' which further dissociates into the products Al_{n-4}^- and $2Al_2O$.

Thus, in accordance with our experiments, the large exothermic energies calculated for primary steps of all the spin-allowed processes is reflected in fast reactions (eqn (19, 20a–c)). In contrast, for the spin-forbidden reactions (*e.g.* eqn (18)), we have a two-fold control of kinetics. Firstly, starting from the ground state of the triplet primary product, the system must provide enough energy to reach the crossing point of the triplet/singlet PES, *i.e.* surmount an energy barrier;§§§ and, secondly, the spin flip, a very unlikely process for these clusters, has to proceed (*cf.* above). Therefore, spin-forbidden reactions can be slowed down for different reasons. Particularly stable systems such as Al_{13}^- do not release the required amount of energy upon educt formation (−0.36 eV), and therefore both factors (barrier + spin flip) may be responsible for the slow reaction rate that is observed. In contrast, the spin-forbidden reaction of $^{\downarrow\uparrow}Al_{14}H^-$, like most less stable $Al_{even}H^-$ clusters, releases sufficient energy upon initial product formation (*e.g.* $^{\uparrow\uparrow}[HAl_{14}O_2]^-$, −1.43 eV) easily to overcome the energy barrier where the unlikely transition between the two spin surfaces can occur; the kinetics are therefore entirely governed by the slow spin-flip process.

Finally, we were able to trace the observed inertness of Al_{13}^- clusters in a triplet O_2 atmosphere back to a consequence of spin conservation restrictions. This result obtained

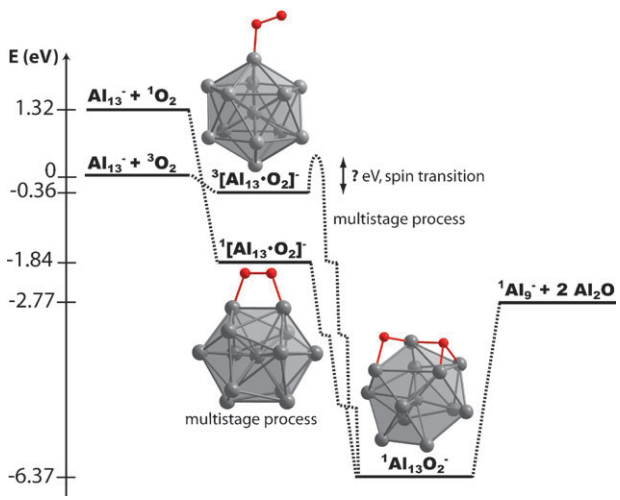

Fig. 11 Energy diagram for the interaction of $^{\downarrow\uparrow}O_2$ and $^{\uparrow\uparrow}O_2$ on the Al_{13}^- cluster surface. The transition from $^{\uparrow\uparrow}[Al_{13}{\cdot}O_2]^-$ to $^{\downarrow\uparrow}Al_{13}O_2^-$ is estimated to be a multi-stage process where O_2 is bound side-on first, then end-on, and then the O–O bond is disrupted; new Al–O bonds are formed (μ^3) and also the spin state changes from triplet to singlet. In addition, the further degradation to Al_9^- and two Al_2O molecules is displayed.

§§§ There is a lack of reliable methods to calculate the height of this barrier. However, for similar reactions in organic chemistry, it is indicated to be 0.8 eV.[79,80]

via FT-ICR mass spectrometry may initiate further experiments in different areas (environmental, biological, medical, material, or energy sciences), where reactions with O_2 are important, and where a proper understanding of primary steps should not be underestimated.

5. The stepwise chlorination of a structurally characterized metalloid cluster, $[Ga_{13}(GaR)_6]^-$, (R = $C(SiMe_3)_3$) and its unexpected reaction products[81,82]

In section 3.2 we introduced the metalloid cluster $[Ga_{13}(GaR)_6]^-$ and demonstrated its stepwise fragmentation after collisionally induced dissociation. To continue investigations on this metalloid cluster compound, we exposed gaseous $[Ga_{13}(GaR)_6]^-$ clusters to chlorine at a pressure around 10^{-8} mbar, and followed the reaction products mass spectrometrically. During the reaction of $[Ga_{13}(GaR)_6]^-$ with Cl_2, a daughter ion $[Ga_{12}(GaClR)(GaR)_5]^-$ is formed initially with the loss of GaCl. Remarkably, and in contrast with reactions of the bare aluminium and gallium clusters described above, one of the chlorine atoms remains bound to the metalloid cluster (eqn (21)).¶¶¶

$$
\begin{aligned}
[Ga_{13}(GaR)_6]^- &\xrightarrow[-GaCl]{+Cl_2} [Ga_{12}(GaClR)(GaR)_5]^- \\
&\xrightarrow[-GaCl]{+Cl_2} [Ga_{11}(GaClR)_2(GaR)_4]^- \\
&\xrightarrow[-GaCl]{+Cl_2} [Ga_{10}(GaClR)_3(GaR)_3]^- \\
&\xrightarrow[-GaCl]{+Cl_2} [Ga_{9}(GaClR)_4(GaR)_2]^- \qquad (21) \\
&\xrightarrow[-GaCl]{+Cl_2} [Ga_{8}(GaClR)_5(GaR)]^- \\
&\xrightarrow[-Ga]{} [Ga_{7}(GaClR)_5(GaR)]^- \\
&\xrightarrow[-GaCl]{+Cl_2} [Ga_{6}(GaClR)_6]^-
\end{aligned}
$$

After stepwise reaction with chlorine (with the release of six GaCl moieties and one Ga atom), $[Ga_6(GaClR)_6]^-$ is formed as the final product observed. In order to gain information on the structure of this species, quantum chemical calculations were performed. For Ga_{12} moieties two structural patterns can be considered in principle, namely, clusters with icosahedral Ga_{12} units or clusters with an octahedral Ga_6 core (metalloid), as displayed in Fig. 12.

Surprisingly, the latter species is favoured by 30 kJ mol^{-1}. This result is unexpected as Wade's Rules[82] predict an icosahedral structural motif. Thus, the metalloid $[Ga_{13}(GaR)_6]^-$ cluster, as a ligand-protected "piece of gallium" (here the Ga_{13}^- cluster), is transformed into another metalloid cluster made up of a Ga_6 core surrounded by six GaR units that are bridged by six chlorine atoms. This unforeseen behaviour can be illustrated by the following picture: a small piece of metal which is coated with a layer of GaR is attacked by Cl_2. While the outer GaR ligand shell with short Ga–Ga bonds to the core remains intact, the Ga atoms of the core are oxidized and GaCl is formed.

¶¶¶ This equation had been incorrectly printed in an earlier paper.[82]

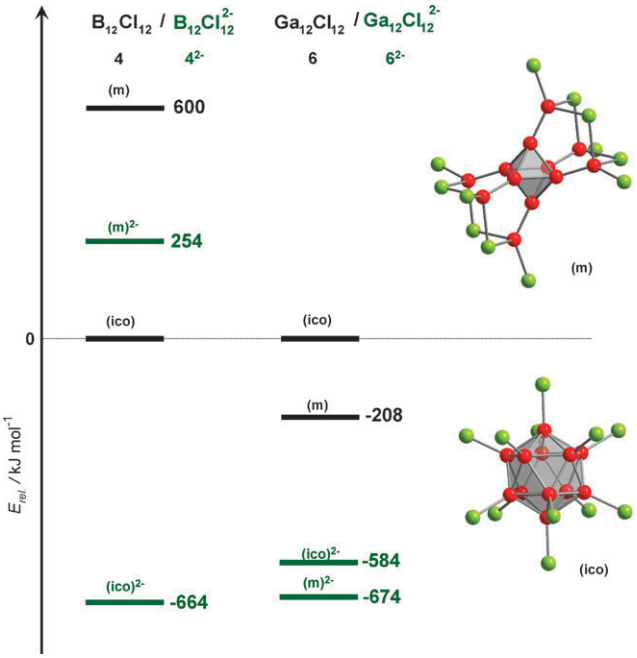

Fig. 12 Energy diagrams show convincingly which structure type is favoured. In the case of boron, the icosahedral (ico) isomers are clearly favoured. Surprisingly, though, the metalloid (m) structure types are preferred in the case of gallium.

Motivated by these findings, we elaborated some fundamental differences between typical Wade-type clusters in boron chemistry and metalloid clusters in gallium chemistry by DFT calculations on neutral and dianionic $[M_{12}Cl_{12}]^{0,2-}$ (M = B, Ga) compounds. For each species we calculated the energies of the isomer with an icosahedral structure and terminally bound ligands (ico) and of the isomer with an octahedral core of naked metal atoms (hence the term "metalloid" (m)). The metalloid clusters have a protecting shell consisting of doubly oxidized MX_2 units; furthermore, bridging (M–X–M) units contribute to the stabilization of the cluster. The energetic relations between all the isomers are displayed in Fig. 12.

Generally, the energetic differences between icosahedral (ico) and metalloid (m) isomers are much more pronounced in the case of boron than in the case of gallium, but in an inverse manner. For boron clusters, the icosahedral isomers are strongly favoured (600 kJ mol^{-1} for the neutral and 918 kJ mol^{-1} for the dianionic species). For gallium clusters, on the other hand, the metalloid isomers prove to be energetically more stable by 65 kJ mol^{-1} and 208 kJ mol^{-1}, respectively. These findings correspond to the experimental results for M_{12} clusters in crystalline compounds. Thus, $[B_{12}F_{12}]^{2-}$ and $[B_{12}H_{12}]^{2-}$ cluster ions[83] contain only halogens terminally bonded to an icosahedral framework. Neutral polyhedral boron subhalides with terminally bonded halogen atoms are also known, *e.g.* B_9Cl_9[84] and B_4Cl_4. On the other hand, and in accordance with our calculations for boron clusters, metalloid

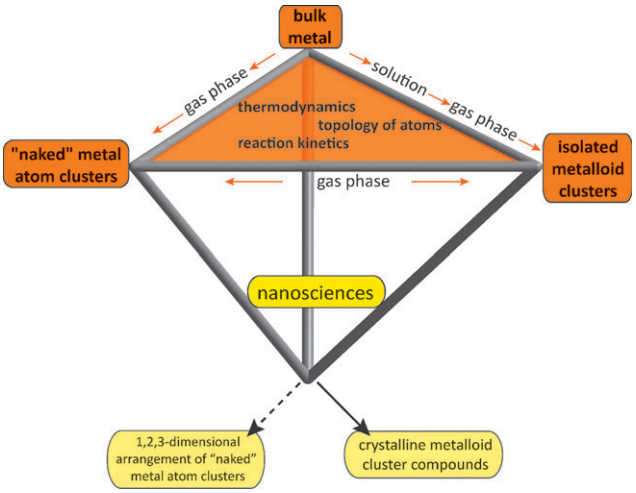

Fig. 13 From the bulk metal *via* naked metal atom clusters and metalloid clusters to nanosciences.

structures that might have been formed after internal disproportionation (*e.g.* $n\mathrm{BX} \rightarrow \mathrm{B}_{n/2}(\mathrm{BX}_2)_{n/2}$) are as yet unknown. The fact that internal disproportionation is preferred for gallium clusters then explains the large number of structurally characterized metalloid gallium clusters, which include the neutral $Ga_{24}Br_{22}$ subhalide $[Ga_{12}(GaBr_2)_{10}(GaBr)_2]$[85] and the analogue $Ga_{24}Br_{18}Se_2$,[86] or the dianionic cluster $[Ga_{12}(GaRBr)_{10}]^{2-}$ (R = $N(SiMe_3)_2$).[87] The centres of all these compounds consist of an icosahedral Ga_{12} core.‡

6. Summary and outlook

The experimental and quantum chemical results presented here clearly demonstrate that the three types of metal–metal bonded species—"naked" metal atom clusters, metalloid clusters, and the bulk metal—have to be discussed together under a common aspect in order to gain a comprehensive overview of metal–metal bonding, chemical reactivity, and characteristic features of the topology of the atoms in each of these three fields. In Fig. 13, the inter-relations between these fields are visualized.

In addition to these relations between isolated clusters ("naked" metal atom clusters and metalloid clusters) and the bulk metal, Fig. 13 also includes one of the final objectives of nanoscience, that is, the arrangement of these clusters as a well-ordered collective, *e.g.* in a crystal, thereby affording what should be a more profound understanding of the interactions between nanoscale clusters.

By means of FT-ICR mass spectrometry it has been possible for the first time to study single metalloid clusters which have been structurally characterized before *via* experimental as well as *via* quantum chemical methods. These experiments show that from a single metalloid cluster (a) a "naked" metal atom cluster can be formed by collisionally induced dissociation, and (b) a smaller metalloid cluster can be obtained *via* a chemical reaction (*e.g.* with Cl_2). On the other hand, the reverse reaction ("naked" metal atom cluster to metalloid cluster) could be made comprehensible *via* single steps. Thus, it has been possible to detect a sequence of reaction steps between a "naked" metal atom cluster ion and an oxidizing molecule (*e.g.* Cl_2, O_2, HCl). With the help of quantum chemical calculations (energetic relations between intermediates) and considering the time-dependent concentration of each intermediate, it has been possible to gain information about the rate constants of chemical reactions for nanoscale metal atom clusters for the first time. This primary quantification of the chemical reactivity of metal atom clusters has to be enlarged in current investigations.

These gas phase investigations by means of FT-ICR mass spectrometry demonstrate that metalloid clusters (*e.g.* $Al_{50}R_{12}$, R = Cp*)[88] ‡can be described either as "naked" metal atom clusters which are oxidized on the outer shell (*e.g.* $Al_{38}(Al^+)_{12}$), or as "naked" metal atom clusters which are stabilized by carbenoid AlR ligands (*e.g.* $Al_{38}(AlR)_{20}$). All the results obtained from reactions of single cluster species in the gas phase—thermodynamics of single steps and change of topology of the metal atoms—demonstrate that there are convincing analogies to reactions of the bulk metal which serve as a reference point with respect to the topology of the atoms and to the energetic situation. Therefore, these gas phase investigations of single clusters afford a first atomistic view of the very complex formation and dissolution processes of the bulk metal.‖‖‖ Even detailed aspects, like the spin conservation rule during reactions with O_2, indicate significant similarities concerning the reaction behaviour of "naked" aluminium atom clusters and the bulk metal. The first investigations of reactions between singlet O_2 and single metal atom clusters should surely initiate further experimental activities by applying FT-ICR methods in areas like biosciences (oxidation of biologically significant macromolecules, *e.g.* after proteolysis), environmental sciences (*e.g.* oxidation of persistent compounds), and materials sciences (*e.g.* corrosion). Such investigations may be expected to provide an insight into the primary steps of O_2 reactions, representing one of the most important reactions of all.

All the results obtained for single clusters not only constitute the basis for understanding the dissolution and formation process of the bulk metal itself, but also lead directly to nanoscience. By taking into account these fundamental results derived *via* FT-ICR mass spectrometry and quantum chemical calculations, tailor-made nanoscopic metal atom clusters, *i.e.* "naked" as well as metalloid cluster compounds, can be obtained and then combined in an assembly of monodisperse entities. Whereas well-ordered collectives (*e.g.* of Al_{13}^- ions; $Al_{13}^-K^+$ has already been discussed as a hypothetical crystalline substance[89]) may be a dream of the future, the synthesis, as well as the one-, two-, or three-dimensional arrangement of monodisperse "naked" metal atom clusters of precious metals, becomes more realistic.[14]** These clusters, like the precious metals themselves, are easier to prepare and to handle than the analogous base metals, since the metal–metal bonds in a cluster of the precious metal are stronger than the

‖‖‖ These "simple" surface reactions also cast light on the complexity of reaction steps during catalytic processes where metal surfaces are involved. Investigations with metal atom clusters as molecular models may be able to elucidate a more localized vision of these processes which take place within the atomic range.

metal–ligand bonds, *i.e.* this behaviour is the opposite of the one found in clusters of base metals.

The reaction conditions under which we have synthesized metalloid Al and Ga clusters during the past decade are obviously ideal in order:

1. to form monodisperse metalloid cluster species on a nanometre scale, and

2. to obtain a perfect arrangement of these species in crystalline compounds.

In addition to the crystalline compounds containing $Ga_{19}R_6$ ($R = C(SiMe_3)_3$)[4] (Fig. 3) and $Al_{50}Cp^*_{12}$[88] moieties already mentioned, we have investigated particularly crystals containing the largest metalloid cluster species (with respect to the "naked" metal atoms), *viz*. $Ga_{84}R_{20}^{4-}$ ($R = N(SiMe_3)_2$.[90,91]‡ The conclusion of 5 years of intense investigation of the electrical conductivity and superconductivity of this crystalline compound seems to be a disillusion for nanoscience.[92–98] Only the perfect arrangement of nanoscale clusters will result in the special intercluster interactions necessary for these electron transport phenomena. Minuscule changes of the cluster orientation within the crystal lattice already prevent electron transport because of the disturbance of the cluster–cluster interactions. However, this disillusionment applies mainly to the preparation of nanoscale materials by means of physical methods (*e.g.* lithographic processes). On the other hand, the realization of perfection is a central challenge for chemical activities, as the results for the Ga_{84} compound dramatically demonstrate. In order to plan chemical work on nanoscale materials under these conditions, therefore, the results presented in this paper may advance some fundamental ideas.

Acknowledgements

We thank the Deutsche Forschungsgemeinschaft, the Centre for Functional Nanostructures (CFN), and the Fonds der Chemischen Industrie for financial support. Special thanks to P. Hauser (for the cover picture), M. Kayas, and S. Schneider for essential help in preparing this manuscript and the figures.

References

1 F. A. Cotton, *Inorg. Chem.*, 1964, **3**, 1217–1220.
2 F. A. Cotton, *Q. Rev. Chem. Soc.*, 1966, **20**, 389–401.
3 A. Purath, R. Köppe and H. Schnöckel, *Angew. Chem., Int. Ed.*, 1999, **38**, 2926–2928.
4 A. Schnepf, G. Stößer and H. Schnöckel, *J. Am. Chem. Soc.*, 2000, **122**, 9178–9181.
5 A. Schnepf and H. Schnöckel, *Angew. Chem., Int. Ed.*, 2002, **41**, 3532–3554.
6 H. Schnöckel and H. Köhnlein, *Polyhedron*, 2002, **21**, 489–501.
7 H. Schnöckel and A. Schnepf, *Adv. Organomet. Chem.*, 2001, **47**, 235–281.
8 H. Schnöckel and A. Schnepf, *ACS Symp. Ser.*, 2002, **822**, 154–167.
9 H. Schnöckel, *Dalton Trans.*, 2005, 3131–3136.
10 G. Linti, H. Schnöckel, W. Uhl and N. Wiberg, in *Clusters of the Heavier Group 13 Elements*, ed. M. Drieß and H. Nöth, Wiley-VCH, Weinheim, 2004, pp. 126–168.
11 C. Dohmeier, D. Loos and H. Schnöckel, *Angew. Chem., Int. Ed. Engl.*, 1996, **35**, 129–149.
12 A. Ecker, E. Weckert and H. Schnöckel, *Nature*, 1997, **387**, 379–381.
13 X. G. Gong, D. Y. Sun and X.-Q. Wang, *Phys. Rev. B: Condens. Matter Mater. Phys.*, 2000, **62**, 15413–15416.
14 E. G. Mednikov, M. C. Jewell and L. F. Dahl, *J. Am. Chem. Soc.*, 2007, **129**, 11619–11630.
15 R. L. Whetten and R. C. Price, *Science*, 2007, **318**, 407–408.
16 P. D. Jadzinsky, G. Calero, C. J. Ackerson, D. A. Bushnell and R. D. Kornberg, *Science*, 2007, **318**, 430–433.
17 H. Schnöckel, *Dalton Trans.*, 2008, DOI: 10.1039/b718784j.
18 K. Wade, *Adv. Inorg. Chem. Radiochem.*, 1976, **18**, 1–66.
19 D. M. P. Mingos, *Nature*, 1972, **236**, 99–102.
20 R. E. Williams, *Chem. Rev.*, 1992, **92**, 177–207.
21 K. Weiss and H. Schnöckel, *Z. Anorg. Allg. Chem.*, 2003, **629**, 1175–1183.
22 R. Burgert, K. Koch, H. Schnöckel, M. Weisser, H.-J. Meyer and H. G. von Schnering, *Angew. Chem., Int. Ed.*, 2004, **44**, 265–269.
23 O. Treutler and R. Ahlrichs, *J. Chem. Phys.*, 1995, **102**, 346–354.
24 A. D. Becke, *Phys. Rev. A: At., Mol., Opt. Phys.*, 1988, **38**, 3098–3100.
25 J. P. Perdew, *Phys. Rev. B: Condens. Matter Mater. Phys.*, 1986, **33**, 8822–8824.
26 K. Eichkorn, O. Treutler, H. Oehm, M. Haeser and R. Ahlrichs, *Chem. Phys. Lett.*, 1995, **240**, 283–290.
27 K. Eichkorn, F. Weigend, O. Treutler and R. Ahlrichs, *Theor. Chem. Acc.*, 1997, **97**, 119–124.
28 A. Schaefer, H. Horn and R. Ahlrichs, *J. Chem. Phys.*, 1992, **97**, 2571–2577.
29 M. Binnewies and E. Milke, *Thermochemical Data of Elements and Compounds*, Wiley VCH, Weinheim, 2002, vol. 2.
30 R. Ahlrichs and S. D. Elliott, *Phys. Chem. Chem. Phys.*, 1999, **1**, 13–21.
31 T. Baer and W. L. Hase, *Unimolecular Reaction Dynamics: Theory and Experiments*, Oxford University Press, New York, 1996.
32 M. Olzmann, H. Schnöckel and R. Burgert, *J. Chem. Phys.*, 2008, manuscript in preparation.
33 M. Olzmann and J. Troe, *Ber. Bunsen-Ges. Phys. Chem.*, 1992, **96**, 1327–1332.
34 K. Weiss and H. Schnöckel, *Anal. Bioanal. Chem.*, 2003, **377**, 1098–1101.
35 K. Koch, R. Burgert, G. Stößer and H. Schnöckel, *Eur. J. Mass Spectrom.*, 2005, **11**, 469–474.
36 Y. Q. Zheng, H. G. von Schnering, J. H. Chang, Y. Grin, G. Engelhardt and G. Heckmann, *Z. Anorg. Allg. Chem.*, 2003, **629**, 1256–1264.
37 E. J. Welch, N. R. M. Crawford, R. G. Bergman and J. R. Long, *J. Am. Chem. Soc.*, 2003, **125**, 11464–11465.
38 K. Koch, A. Schnepf and H. Schnöckel, *Z. Anorg. Allg. Chem.*, 2006, **632**, 1710–1716.
39 M. Weisser, M. Ströbele and H. J. Meyer, *C. R. Chim.*, 2005, **8**, 1820–1826.
40 M. Weisser, R. Burgert, H. Schnöckel and H.-J. Meyer, *Z. Anorg. Allg. Chem.*, 2008, **634**, 633–640.
41 P. Yang, R. Köppe, T. Duan, J. Hartig, G. Hadiprono, B. Pilawa, I. Keilhauer and H. Schnöckel, *Angew. Chem., Int. Ed.*, 2007, **46**, 3579–3583.
42 S. D. Köhler, B. Pilawa, D. S. d. Jauregui, G. Fischer, R. Köppe, A. Schnepf, H. Schnöckel and E. Dormann, *Europhys. Lett.*, submitted.
43 K. Weiss, R. Köppe and H. Schnöckel, *Int. J. Mass Spectrom.*, 2002, **214**, 383–395.
44 H. Köhnlein, A. Purath, C. Klemp, E. Baum, I. Krossing, G. Stößer and H. Schnöckel, *Inorg. Chem.*, 2001, **40**, 4830–4838.
45 C. Klemp, M. Bruns, J. Gauss, U. Haeussermann, G. Stößer, L. van Wuellen, M. Jansen and H. Schnöckel, *J. Am. Chem. Soc.*, 2001, **123**, 9099–9106.
46 C. Klemp, R. Köppe, E. Weckert and H. Schnöckel, *Angew. Chem., Int. Ed.*, 1999, **38**, 1740–1743.
47 M. F. Jarrold, J. E. Bower and J. S. Kraus, *J. Chem. Phys.*, 1987, **86**, 3876–3885.
48 M. F. Jarrold and J. E. Bower, *J. Am. Chem. Soc.*, 1988, **110**, 6706–6716.
49 R. E. Leuchtner, A. C. Harms and A. W. Castleman, Jr, *J. Chem. Phys.*, 1991, **94**, 1093–1101.
50 K. Kaya, K. Fuke, S. Nonose and N. Kikuchi, *Z. Phys. D: At., Mol. Clusters*, 1989, **12**, 571–573.

51 D. E. Bergeron, A. W. J. Castleman, T. Morisato and S. N. Khanna, *Science*, 2004, **304**, 84–87.
52 D. E. Bergeron, P. J. Roach, A. W. Castleman, N. Jones and S. N. Khanna, *Science*, 2005, **307**, 231–235.
53 A. F. Holleman, E. Wiberg and N. Wiberg, *Lehrbuch der Anorganischen Chemie*, De Gruyter, Berlin, 2007.
54 W. D. Knight, W. A. De Heer, W. A. Saunders, K. Clemenger, M. Y. Chou and M. L. Cohen, *Chem. Phys. Lett.*, 1987, **134**, 1–5.
55 B. K. Rao and P. Jena, *J. Chem. Phys.*, 1999, **111**, 1890–1904.
56 W. D. Knight, K. Clemenger, W. A. De Heer, W. A. Saunders, M. Y. Chou and M. L. Cohen, *Phys. Rev. Lett.*, 1984, **52**, 2141–2143.
57 M. Brack, *Rev. Mod. Phys.*, 1993, **65**, 677–732.
58 W. A. de Heer, *Rev. Mod. Phys.*, 1993, **65**, 611–676.
59 R. Burgert, H. Schnoeckel, M. Olzmann and K. H. Bowen, Jr., *Angew. Chem., Int. Ed.*, 2006, **45**, 1476–1479.
60 A. G. Marshall, T. C. L. Wang and T. L. Ricca, *J. Am. Chem. Soc.*, 1985, **107**, 7893–7897.
61 P. Langevin, A Fundamental Formula of Kinetic Theory, *Ann. Chim. Phys.*, 1905, **5**, 245–288.
62 J. I. Steinfeld, J. S. Francisco and W. L. Hase, *Chemical Kinetics Dynamics*, Prentice Hall, Upper Saddle River, New Jersey, 2nd edn, 1999.
63 A. Purath, C. Dohmeier, A. Ecker, R. Köppe, H. Krautscheid, H. Schnöckel, R. Ahlrichs, C. Stoermer, J. Friedrich and P. Jutzi, *J. Am. Chem. Soc.*, 2000, **122**, 6955–6959.
64 S. A. Ruatta, L. Hanley and S. L. Anderson, *Chem. Phys. Lett.*, 1987, **137**, 5–9.
65 C. Dohmeier, D. Loos and H. Schnöckel, *Angew. Chem., Int. Ed. Engl.*, 1996, **35**, 129–149.
66 R. Burgert, S. T. Stokes, K. H. Bowen and H. Schnöckel, *J. Am. Chem. Soc.*, 2006, **128**, 7904–7908.
67 R. Burgert, H. Schnöckel, A. Grubisic, X. Li, S. T. Stokes, G. F. Ganteför, B. Kiran, P. Jena and K. H. Bowen, *Science*, 2008, **319**, 438–442.
68 T. P. Martin, *Phys. Rep.*, 1996, **273**, 199–241.
69 J. Behler, B. Delley, S. Lorenz, K. Reuter and M. Scheffler, *Phys. Rev. Lett.*, 2005, **94**, 036104/1-4.
70 P. S. Bagus, C. R. Brundle, F. Illas, F. Parmigiani and G. Polzonetti, *Phys. Rev. B: Condens. Matter Mater. Phys.*, 1991, **44**, 9025–9034.
71 I. P. Batra and L. Kleinman, *J. Electron Spectrosc. Relat. Phenom.*, 1984, **33**, 175–241.
72 J. Z. Sexton and A. C. Kummel, *J. Chem. Phys.*, 2004, **121**, 6518–6524.
73 M. Binetti, O. Weisse, E. Hasselbrink, G. Katz, R. Kosloff and Y. Zeiri, *Chem. Phys. Lett.*, 2003, **373**, 366–371.
74 A. J. Komrowski, H. Ternow, B. Razaznejad, B. Berenbak, J. Z. Sexton, I. Zoric, B. Kasemo, B. I. Lundqvist, S. Stolte, A. W. Kleyn and A. C. Kummel, *J. Chem. Phys.*, 2002, **117**, 8185–8189.
75 H. Schwarz, *Int. J. Mass Spectrom.*, 2004, **237**, 75–105.
76 X. Li, A. Grubisic, S. T. Stokes, J. Cordes, G. F. Ganteför, K. H. Bowen, B. Kiran, M. Willis, P. Jena, R. Burgert and H. Schnöckel, *Science*, 2007, **315**, 356–358.
77 A. C. Reber, S. N. Khanna, P. J. Roach, W. H. Woodward and A. W. Castleman, *J. Am. Chem. Soc.*, 2007, **129**, 16098–16101.
78 R. Ahlrichs, C. Ehrhardt, M. Lakenbrink, S. Schunck and H. Schnöckel, *J. Am. Chem. Soc.*, 1986, **108**, 3596–3602.
79 W. Adam, *Chem. Unserer Zeit*, 1981, **15**, 190–196.
80 A. Greer, *Acc. Chem. Res.*, 2006, **39**, 797–804.
81 K. Koch and H. Schnöckel, *Z. Anorg. Allg. Chem.*, 2007, **633**, 873–878.
82 K. Koch, R. Burgert and H. Schnoeckel, *Angew. Chem., Int. Ed.*, 2007, **46**, 5795–5798.
83 S. V. Ivanov, S. M. Miller, O. P. Anderson, K. A. Solntsev and S. H. Strauss, *J. Am. Chem. Soc.*, 2003, **125**, 4694–4695.
84 H. Binder, R. Kellner, K. Vaas, M. Hein, F. Baumann, M. Wanner, R. Winter, W. Kaim, W. Honle, Y. Grin, U. Wedig, M. Schultheiss, R. K. Kremer, H. G. Von Schnering, O. Groeger and G. Engelhardt, *Z. Anorg. Allg. Chem.*, 1999, **625**, 1059–1072.
85 T. Duan, E. Baum, R. Burgert and H. Schnöckel, *Angew. Chem., Int. Ed.*, 2004, **43**, 3190–3192.
86 J. Hartig, F. Klöwer, J. Rinck, A.-N. Unterreiner and H. Schnöckel, *Angew. Chem., Int. Ed.*, 2007, **46**, 6549–6552.
87 A. Schnepf, R. Köppe, E. Weckert and H. Schnöckel, *Chem.–Eur. J.*, 2004, **10**, 1977–1981.
88 J. Vollet, J. R. Hartig and H. Schnöckel, *Angew. Chem., Int. Ed.*, 2004, **43**, 3186–3189.
89 W. J. Zheng, O. C. Thomas, T. P. Lippa, S. J. Xu and K. H. Bowen, Jr, *J. Chem. Phys.*, 2006, **124**, 144304/1-5.
90 A. Schnepf and H. Schnöckel, *Angew. Chem., Int. Ed.*, 2001, **40**, 712–715.
91 A. Schnepf, B. Jee, H. Schnöckel, E. Weckert, A. Meents, D. Luebbert, E. Herrling and B. Pilawa, *Inorg. Chem.*, 2003, **42**, 7731–7733.
92 J. Hagel, M. T. Kelemen, G. Fischer, B. Pilawa, J. Wosnitza, E. Dormann, H. von Loehneysen, A. Schnepf, H. Schnöckel, U. Neisel and J. Beck, *J. Low Temp. Phys.*, 2002, **129**, 133–142.
93 O. N. Bakharev, N. Zelders, H. B. Brom, A. Schnepf, H. Schnöckel and L. J. de Jongh, *Eur. Phys. J. D*, 2003, **24**, 101–104.
94 O. N. Bakharev, D. Bono, H. B. Brom, A. Schnepf, H. Schnöckel and L. J. de Jongh, *Phys. Rev. Lett.*, 2006, **96**, 117002/1-4.
95 D. Bono, A. Schnepf, J. Hartig, H. Schnöckel, G. J. Nieuwenhuys, A. Amato and L. J. de Jongh, *Phys. Rev. Lett.*, 2006, **97**, 077601-1-4.
96 J. Frenzel, S. Gemming and G. Seifert, *Phys. Rev. B: Condens. Matter Mater. Phys.*, 2004, **70**, 235404/1-8.
97 J. Hartig, A. Schnepf, J. de Jongh, D. Bono and H. Schnöckel, *Z. Anorg. Allg. Chem.*, 2007, **633**, 63–76.
98 D. Bono, O. N. Bakharev, A. Schnepf, J. Hartig, H. Schnöckel and L. J. de Jongh, *Z. Anorg. Allg. Chem.*, 2007, **633**, 2173–2177.